

African dust transported to Barbados in the Wintertime Lacks Indicators of Chemical Aging

Haley M. Royer^{1,2}, Michael T. Sheridan^{1,3}, Hope E. Elliott⁴, Edmund Blades¹, Nurun Nahar Lata⁵, Zezhen Cheng⁵, Swarup China⁵, Zihua Zhu⁵, Andrew P. Ault⁶, Cassandra J. Gaston^{1*}

¹Department of Atmospheric Sciences, Rosenstiel School of Marine, Atmospheric, and Earth Science, University of Miami, Miami, FL

²Currently at: Department of Environmental Sciences and Engineering, University of North Carolina at Chapel Hill, Chapel Hill, NC

³Skidaway Institute of Oceanography, University of Georgia, Athens, GA

⁴Department of Ocean Sciences, Rosenstiel School of Marine, Atmospheric, and Earth Science, University of Miami, Miami, FL

⁵Environmental Molecular Sciences Laboratory, Pacific Northwest National Laboratory, Richland, WA

⁶Department of Chemistry, University of Michigan, Ann Arbor, MI

*Corresponding Author:

Cassandra J. Gaston: Email: cgaston@miami.edu, Phone: (305)-421-4979

1. Abstract

The chemical processing (“aging”) of mineral dust is thought to increase dust light scattering efficiency, cloud droplet activation, and nutrient solubility. However, the extent of African dust aging during long-range transport to the western Atlantic is poorly understood. Here, we explore African dust aging in wintertime samples collected from Barbados when dust is transported at lower altitudes. Ion chromatography (IC) analysis indicates that the mass concentrations of bulk nitrate, sulfate, and oxalate increase, relative to background conditions, when African dust reaches Barbados after transatlantic transport, indicating dust aging. However, aerosol mixing state analysis from computer-controlled scanning electron microscopy with energy dispersive x-ray spectroscopy (CCSEM/EDX) indicates that approximately 67% of dust particles are internally mixed with sea salt, while only about 26% of dust particles contain no internally mixed components. SEM/EDX elemental mapping and time-of-flight secondary ion mass spectrometry (TOF-SIMS) reveals that within internally mixed dust and sea salt particles, only sea salt components contain signs of aging as indicated by the loss of chloride and acquisition of nitrate and/or sulfate. Our results suggest that chemical aging may only modestly increase the solubility of nutrients in African dust during long range transport. Because most dust that we measured was internally mixed with sea salt, chemical aging is not necessarily required to increase the hygroscopicity of dust, at least in the lower boundary layer. Further, our findings have implications for understanding the release of halogens from sea salts, which may be enhanced in internally mixed dust and sea salt particles.

2. Introduction

Upon emission, dust can directly scatter or absorb solar radiation (Balkanski et al., 2007; Haywood et al., 2003; Myhre & Stordal, 2001; Sokolik et al., 2001; Tegen, 2003), act as cloud condensation (Albrecht, 1989; Koehler et al., 2009; Levin et al., 1996; Rosenfeld et al., 2001) and ice nuclei (Archuleta et al., 2005; Cziczo et al., 2004; DeMott et al., 2003), and provide micro- and macro- nutrients to nutrient-limited ecosystems (Elliott et al., 2024; Jickells et al., 2005; Mahowald, 2011). However, mineral dust aerosol is still poorly represented in climate models due, in part, to a lack of understanding of the physiochemical properties of dust and their changes as a result of cloud processing (Gierlus et al., 2012; Wurzler et al., 2000), multiphase reactions (Andreae et al., 1986; Sullivan et al., 2007; Sullivan & Prather, 2007) or heterogeneous reactions with polluted air masses (Fitzgerald et al., 2015; Krueger et al., 2004; Sullivan et al., 2009). The chemical change in the physiochemical properties of dust due to heterogeneous or multiphase reactions, herein referred to as “aging”, can alter the water uptake properties of dust (Krueger et al., 2003; Laskin et al., 2005) thus affecting its light scattering efficiency (Bauer et al., 2007; Kandler et al., 2011; Levin et al., 1996), cloud droplet activation properties (Gibson et al., 2007; Kelly et al., 2007; Sullivan et al., 2009; Tang et al., 2016), and atmospheric lifetime (Abdelkader et al., 2015; Lance et al., 2013; Li et al., 2014; Wu et al., 2013). We note that chemical aging is distinct from other changes in the physicochemical properties of dust that may occur during transport such as coagulation. Chemical aging is also essential to increase the bioavailability of nutrients within dust via ligand-mediated and proton-mediated dissolution processes (Nenes et al., 2011; Spokes & Jickells, 1995; Stockdale et al., 2016). Modeling the chemical aging process is challenging and, as a result, models often treat dust as a chemically

homogeneous and hydrophobic particle type (Han et al., 2011; Pringle et al., 2010; Shi et al., 2008), which oversimplifies the complexity of dust and its impacts in the atmosphere.

African dust is the largest source of dust, which is transported to the Caribbean, North and South America and Europe (Barkley et al., 2019; Prospero & Mayol-Bracero, 2013). Most research studying African dust transport focuses on the summer when dust mass concentrations are at a maximum (Prospero & Mayol-Bracero, 2013; Zuidema et al., 2019) and the Saharan Air Layer (SAL) that transports dust across the Atlantic is at its maximum altitude (Carlson & Prospero, 1972). The height of African dust transport minimizes the mixing time of transported dust with the underlying Marine Boundary Layer (MBL) until the dust settles out of the SAL (Ryder et al., 2018). Studies exploring African dust aging during the summertime have produced varying results. Early attempts to study dust aging in the western Atlantic from Li-Jones & Prospero, 1998, found a strong correlation between mineral dust and non-sea salt sulfate (NSS- SO_4^{2-}) from size-resolved filter measurements collected in Barbados during the boreal spring, which they conclude is the result of dust aging by sulfur emissions from Europe. In a more recent study from Izaña, African dust has been shown to acquire sulfate from industrial emissions from North Africa (Rodriguez et al., 2011). Further, single-particle methods have been utilized to obtain more detail on the mixing state of dust to unambiguously determine if markers of aging are located within dust or other aerosol particles. Conclusions from Denjean et al., 2015, inferred from low hygroscopicity growth measurements, that long range transported African dust particles collected over Puerto Rico in the boreal summer are not chemically processed and are minimally mixed with other chemical components. In contrast, iron solubility was found to increase in Saharan dust during transatlantic transport, in part, due to chemical aging (Rodriguez et al., 2021). Further, Fitzgerald et al., 2015 also analyzed long range transported African dust in

Puerto Rico during the boreal summer, but found sulfate and oxalate on dust particles using real-time single-particle mass spectrometry. Dust composition measured by Fitzgerald et al., 2015 may have also been affected by local cloud processing as sampling occurred within a cloud forest. Boreal summer analysis of long range transported dust in Barbados from Kandler et al., 2018 and Weinzierl et al., 2017 revealed limited aging of dust particles with some internal mixing with other chemical components from microscopy and spectroscopy analysis. Model analysis of summertime African dust transport from Abdelkader et al., 2017 explored the evolution of dust aging as dust is transported from Africa to the western Atlantic, finding that aged African dust is quickly removed from the aerosol loading during transit across the Atlantic, leaving minimally-aged dust within the aerosol loading that reaches the western Atlantic.

Unlike the summertime when dust is transported within the elevated SAL, dust is transported at lower altitudes during the wintertime (Tsamalis et al., 2013) enhancing the mixing time of dust within the MBL, which may increase the interaction between dust, anthropogenic emissions, and marine biogenic emissions in the MBL (Gutleben et al., 2022; Savoie & Prospero, 1982). In addition to anthropogenic emissions that mix with dust (Gaston et al., 2024; Rodriguez et al., 2011), the Sahelian burn season occurs during the boreal winter, often resulting in long-range co-transport of dust and smoke emissions that were specifically observed during the ATOMIC/EUREC⁴A campaigns (Quinn et al., 2021; Royer et al., 2023). Smoke emissions are known to contain sulfur dioxide (SO₂) and nitrogen oxides (e.g., NO_x≡NO + NO₂) that theoretically could age dust extensively (Hickman et al., 2021; Rickly et al., 2022), especially during long-range transport in which dust has several days to interact with smoke emissions before it arrives in the western Atlantic. During the ATOMIC/EUREC⁴A campaigns, sulfate was observed on smoke particles, indicating a potential for dust aging during co-transport with smoke

(Royer et al., 2023). However, the likelihood of mixing between the emissions in the MBL, dust, and African smoke emissions and their impact on dust aging during the wintertime is unclear.

The goal of this study is to determine the extent of aging on African dust particles transported to the Caribbean during the boreal winter using methods that determine the mixing state of individual particles. Collection of aerosol samples took place at the Barbados Atmospheric Chemistry Observatory (BACO) at Ragged Point, Barbados from January through February of 2020 during the ATOMIC/EUREC⁴A campaign. During the sampling period, 3 dust events consisting of co-transported dust and smoke originating from Africa arrived at Barbados, offering ample opportunity to study the extent of aging. Lidar measurements also reveal that dust-laden air masses remained at a low altitude (3.5 km) for the duration of their transit to Ragged Point, contrasting high altitude summertime transport conditions (Gutleben et al., 2022). This study provides a unique opportunity for exploring the extent of dust aging on African dust, which should be at a maximum under the conditions described. Our findings provide much needed insight into the extent of aging for African aerosols undergoing long range transport to the western Atlantic, which is essential for properly modeling the water uptake properties of dust particles in the atmosphere as well as the solubility of nutrients in dust bearing minerals.

3. Methods

3.1 Measurement Site and Sampling Period

The sampling site, sampling period, and air mass origins that were studied have been described previously in Royer et al., 2023. Briefly, aerosol samples consisting of long-range co-transported African dust and smoke as well as marine aerosols were collected at the University of Miami's Barbados Atmospheric Chemistry Observatory (BACO) at Ragged Point during the EUREC⁴A and ATOMIC campaigns from 20 January through 20 February 2020 (Quinn et al.,

2021; Stevens et al., 2021). Air mass origins were determined using NOAA's HYSPLIT model as well as daily dust mass concentrations (Stein et al., 2015). Ragged Point (13°6' N, 59°37'W), a prominence on Barbados' eastern coast, is an ideal location for studying the extent of dust aging in long range transported African aerosols as it is exposed to the steady easterly trade winds which regularly carry outflows of African aerosols such as dust and smoke to the island (Archibald et al., 2015; Carlson & Prospero, 1972; Prospero, 1968) and minimize the influence of anthropogenic activity from local islands to the west (Prospero et al., 2005; Savoie et al., 2002).

In this study, we utilize both bulk and single-particle methods to highlight the importance of aerosol mixing state for understanding the extent of dust aging. Bulk methods have traditionally been used to study long-range dust transport and the extent of dust aging in the western Atlantic (Chen & Siefert, 2004; Li-Jones & Prospero, 1998; Savoie et al., 2002). Single particle methods used herein show that elucidating the aerosol mixing state is essential for determining the full extent of aging in long range transported African dust particles.

3.2 Mass Concentrations of Dust and Soluble Ion Content

To collect aerosol samples, the BACO is equipped with a high-volume sampler and an isokinetic aerosol inlet on top of a 17 m-tall tower situated on a 30 m bluff along the coast at Ragged Point. Aerosol filters were collected using a high-volume sampler pumping at a rate of approximately 0.7 m³/min for bulk measurements and 1.0 m³/min for size-resolved measurements. Size-resolved filters were collected on a cascade impactor (Tisch Environmental, Inc., Series 230) with 6 stages and 1 backing filter. Size-resolved aerosol analysis are separated into supermicron (stages 1-4; >1.3 µm) and submicron (stages 5 – backing filter; <1.3 µm). All aerosol filter samples were collected on cellulose Whatman-41 (W-41) filters with a nominal 20

µm pore size. After filter collection, filters were washed with Milli-Q water three times to remove soluble material. The washed filters were subsequently combusted in a furnace at 500 °C for about 12 h (i.e., overnight) to remove the cellulose filter and determine daily dust mass concentrations (Prospero et al., 2021; Zuidema et al., 2019). Procedural filter blanks were also collected by placing a filter in the sampler cassette for 15 min without turning on the pump. The resulting ash mass from a sample minus the mass of a filter blank is the gross ash weight, which is then adjusted by a factor of 1.3 to convert the ash weight to a mineral dust concentration (Prospero, 1999; Zuidema et al., 2019).

To determine daily bulk and size-resolved soluble ion content, the 20 mL of Milli-Q used to wash the filters was filtered through a 25 mm membrane filter with 0.4 µm pore size (Whatman Nuclepore Track Etch Membrane) to remove any particulates from the washing process. Filtrate was then frozen in a -20°C freezer until analysis. To prepare samples, frozen filtrate was thawed in a warm water bath and vortexed for 20 sec. The filtrate was then analyzed using an ion chromatography (IC) instrument (Dionex Integrion HPIC System; Thermo Scientific). Samples were analyzed in triplicate to ensure precision of results. To obtain soluble ion content, 5 mL aliquots of filtrate were injected into the IC system and analyzed for cations (IonPac CG12A/CS12A; Thermo Scientific) and anions (IonPac AS11-HC; Thermo Scientific). Cations of interest analyzed by IC include lithium (Li^+), sodium (Na^+), ammonium (NH_4^+), potassium (K^+), magnesium (Mg^+), and calcium (Ca^+) while anions of interest include fluoride (F^-), formate (CH_2O^-), methanesulfonate (MSA), chloride (Cl^-), nitrite (NO_2^-), bromide (Br^-), nitrate (NO_3^-), sulfate (SO_4^{2-}), oxalate, and phosphate (PO_4^{3-}). Since the filtrate analyzed includes sea salt emissions, which may include sulfate from ocean emissions, non-sea salt sulfate (NSS- SO_4^{2-}) was calculated using the equation (Gaston et al., 2024)

$$[NSS - SO_4^{2-}] = [SO_4^{2-}] - (0.2517 * [Na]) \quad (1)$$

to determine the fraction of sulfate derived from non-sea spray emissions including anthropogenic and marine biogenic sources. For the purposes of this study, we focus primarily on $NSS-SO_4^{2-}$ and NO_3^- as they are chemical indicators of dust aging (Sullivan et al., 2007) as well as oxalate as it indicates cloud processing and other processes (Ma et al., 2004). Samples were also analyzed for methanesulfonate, an important tracer of ocean-derived biogenic sulfur (Gaston et al., 2010) that can age dust particles (Desboeufs et al., 2024), however MSA measurements were negligible.

3.3 Aerosol Collection for Single Particle Mixing State Analysis

To determine the mixing state of individual particles, aerosol samples were collected at ambient relative humidity (RH) through an isokinetic aerosol inlet with a three-stage microanalysis particle sampler (MPS-3, California Measurements, Inc.), which samples particles from diameters of 5.0-2.5 μm (stage 1), 2.5-0.7 μm (stage 2), and <0.7 μm (stage 3). For each set of samples (one set including one sample from each stage of the MPS), the MPS was run for 45 min at 2 L/min flow starting at approximately 09:30 LT (local time) or 13:30 coordinated universal time (UTC). Meteorological data from a local station were used to manually check that wind direction fell between 335 and 130 degrees and that wind speeds were greater than 1 m/s during all sampling periods to ensure that only air from the open ocean to the east was sampled rather than local, anthropogenically-influenced air.

3.4 Single Particle Elemental Composition and Particle Source Determined from Computer Controlled Scanning Electron Microscopy Coupled to Energy Dispersive X-ray Spectroscopy (CCSEM-EDX)

To determine aerosol elemental composition, particles were deposited onto carbon-coated copper grids (Ted Pella, Inc., Prod. # 01910-F) on each of the 3 stages of the MPS that were later analyzed at the Environmental Molecular Science Laboratory (EMSL) at Pacific Northwest National Laboratory (PNNL) using computer-controlled scanning electron microscopy (Quanta 3D) coupled with energy-dispersive X-ray spectroscopy (EDAX, Inc.) (CCSEM/EDX). SEM provides images, size, and morphology of individual particles while EDX measures the semi-quantitative elemental composition of each particle. Approximately 1800 particles from stage 1, 2500 particles from stage 2, and 3200 particles from stage 3 were analyzed via CCSEM/EDX for each day of sampling. Only particles with diameters $>0.1 \mu\text{m}$ were analyzed. Semiquantitative data products from CCSEM/EDX analysis were then analyzed in MATLAB (version 9.6.0; The Mathworks, Inc.) using a k-means clustering algorithm (Ault et al., 2012; Royer et al., 2023; Shen et al., 2016) to group similar particles into clusters based on the elemental percentage, size, and shape of individual particles. These clusters are then assigned to particle types based on their morphology, characteristic EDX spectra, and the existing literature. Percent composition threshold values of 1% were used when processing CCSEM/EDX data to ensure the presence of elements detected by the EDX. Single particle analysis using CCSEM/EDX was limited to 16 elements found in common aerosols such as dust, sea salt, and smoke particles: carbon (C), nitrogen (N), oxygen (O), sodium (Na), magnesium (Mg), aluminum (Al), silicon (Si), phosphorus (P), sulfur (S), chlorine (Cl), potassium (K), calcium (Ca), vanadium (V), manganese (Mn), iron (Fe), and nickel (Ni). To prevent the signal from the copper (Cu)-grid from interfering with measuring the other elements in the particles, Cu was intentionally excluded from the list of elements to detect. Though the grids are coated with carbon (C), C was intentionally included due to the presence of organics within the aerosol loading. The inclusion of C may result in a

small underrepresentation of other elements of interest as the C signal may be artificially elevated by the C-coating on the Cu-grids. Commonly used thresholds for detecting an element with CCSEM-EDX are 0.5-1% (by mole fraction) (Hopkins et al., 2008), and depend on factors such as substrate, collection time of spectra, accelerating voltage, sensitivity of the sample to the electron beam, and the element being measured (i.e., EDX is less sensitive to N than S in this analysis). A rough rule of thumb is that when elements are not detected they are < 1% of particle mass.

Particle identification was primarily based on semiquantitative elemental composition determined by EDX. Dust particles were identified based on the presence of elements common in aluminosilicate minerals, including Si, Al, Fe, K, Ca, and Mg detected from EDX analysis (Hand et al., 2010; Krueger et al., 2004; Levin et al., 2005). Sea salt particles were characterized by high Na and Cl content, indicating the presence of halite (NaCl) (Bondy et al., 2018). Smoke particles were identified as containing a combination of C, O, S, and K, as shown previously at this site (Royer et al. 2023) and other sites (Bondy et al. 2018; Olson et al. 2019). Internal mixtures of dust and sea salt contained elements indicative of both dust (Si, Al, Fe, K, Ca, and Mg) and sea salt (Na and Cl), usually with portions of the particle containing primarily dust and other portions containing primarily sea salt. Internally mixed dust and smoke contained elements common in mineral dust as well as high C, K, and S which are representative of carbon-based matter that has undergone combustion and aging from sulfur compounds, leading to the formation of potassium-containing salts (Andreae, 1983; Li et al., 2003).

Analysis of CCSEM/EDX data also included calculating the extent of aging across the aerosol size distribution. To obtain this information, nitrogen (N) and sulfur (S) % values for each particle in a cluster of a known particle type were extracted along with the corresponding

diameter for each particle. Data was then binned according to diameter size, while N and S % values were averaged for each diameter size. Values that did not exceed 1% were rounded down to 0% as only an exceedance of 1% guarantees the presence of an element.

The spatial distribution of elemental components on select particles was also determined using elemental mapping (AZtecLive SmartMapping; Oxford Instruments). Approximately 10 elemental maps were collected for dust, sea salt, and internally mixed dust and sea salt. Spectra were collected for select components within elemental maps to obtain more detailed chemistry across an individual particle, which allows for analysis of sea salt and dust components as well as the extent of aging in these components within internally mixed dust and sea salt particles.

3.5 Determination of the Chemical Composition at the Aerosol Surface using Time-of-Flight Secondary Ion Mass Spectrometry (TOF-SIMS)

The spatial distribution of major ions across the surface of individual particles was also determined. Aerosol particles were collected onto silicon wafers (Ted Pella, Inc., Prod. # 16008) within the MPS, which were then analyzed with time-of-flight secondary ion mass spectrometry (TOF-SIMS; IONTOF GmbH, Munster, Germany) at PNNL (Li et al., 2023). In addition to providing more detailed chemical information on dust aging, TOF-SIMS supplements the time-intensive method of elemental mapping with SEM/EDX by analyzing multiple particles to explore particle aging, thus supporting the representativeness of elemental mapping results to the total aerosol loading (Hopkins et al., 2008). Further, while EDX is limited to elemental data indicative of aging (e.g., the presence of N and/or S), TOF-SIMS can detect compounds such as nitrate (NO_3^-) and sulfate (HSO_4^-) ions that more concretely provide evidence of chemical aging.

To perform TOF-SIMS analysis, a 25 keV Bi_3^+ beam was focused to around a 0.4 μm diameter area on the silicon substrate and scanned over a 100 μm x 100 μm^2 area to produce an

image of 256x256 pixels. The current of the beam was 0.36 pA with 10 kHz pulse frequency, and data collection time was 600 s per set of images. The total ion dose for each sample was under the static limit so that only surface information (<2 nm) was collected for the analyzed particles. Delayed extraction mode was also used during image collection to ensure that both positive and negative ion images could be collected at the exact same location. Ions of interest indicated the presence of sea salt (Na_2Cl^+ and NaCl_2^-), dust (Al^+ and Ca^+), and chemical aging (HSO_4^- and NO_3^-). Surface contamination from the lab space the samples were handled in (e.g., butanediol (m/z -89) likely from butanol used in particle counters in the lab space) was observed in the samples, and to remove contamination, a 20 keV argon (Ar) cluster ($\text{Ar}_{1500\pm300}^+$) sputtering ion beam was used with a beam current of about 2.0 nA before chemical analysis with the 25 keV Bi_3^+ beam occurred. Samples underwent Ar sputtering for 50s to remove the top 100 nm of sample.

4. Results

4.1 Bulk Aerosol Mass Concentrations From Filter Sampling

Figure 1 presents daily dust mass concentrations and bulk soluble ion content along with correlation plots for each ion of interest quantified from our filter samples. Results show a strong correlation between daily dust mass concentrations and nitrate (NO_3^- , $R^2 = 0.75$), dust and non-sea salt sulfate (NSS-SO_4^{2-} , $R^2 = 0.83$), as well as a weak correlation with oxalate ($R^2 = 0.11$) throughout the entire campaign. The presence of nitrate, non-sea salt sulfate, and oxalate from bulk aerosol analysis suggests that dust is being aged during transport. Similar figures for supermicron ($> 1.3 \mu\text{m}$) and submicron ($<1.3 \mu\text{m}$) analysis can be found in Figures S1 and S2, respectively, in the Supporting Information (SI). Notably, dust mass concentrations were evenly split between the supermicron and submicron size modes. Both supermicron (*SUP*) and

submicron (*SUB*) analysis shows similar findings to bulk filter analysis in which a strong correlation exists between dust mass concentrations and nitrate ($R^2_{\text{SUP NO}_3} = 0.50$; $R^2_{\text{SUB NO}_3} = 0.59$), non-sea salt sulfate ($R^2_{\text{SUP NSS-SO}_4} = 0.80$; $R^2_{\text{SUB NSS-SO}_4} = 0.49$), and oxalate ($R^2_{\text{SUP oxalate}} = 0.63$; $R^2_{\text{SUB oxalate}} = 0.27$). Differences between supermicron and submicron analysis indicate that nitrate is more concentrated in the supermicron aerosol loading ($\text{Avg}_{\text{SUP NO}_3} = 0.64 \mu\text{g}/\text{m}^3$; $\text{Avg}_{\text{SUB NO}_3} = 0.44 \mu\text{g}/\text{m}^3$). However, nitrate has an appreciable submicron mode likely due to transported African smoke. Results also show that NSS-SO_4^{2-} ($\text{Avg}_{\text{SUP NSS-SO}_4} = 0.04 \mu\text{g}/\text{m}^3$; $\text{Avg}_{\text{SUB NSS-SO}_4} = 0.46 \mu\text{g}/\text{m}^3$) and oxalate ($\text{Avg}_{\text{SUP oxalate}} = 0.01 \mu\text{g}/\text{m}^3$; $\text{Avg}_{\text{SUB oxalate}} = 0.04 \mu\text{g}/\text{m}^3$) are more concentrated in the submicron aerosol loading (Quinn et al., 2021; Royer et al., 2023; Savoie et al., 1982). These findings suggest that dust is possibly being aged, with supermicron dust being primarily aged by nitrate and submicron dust being primarily aged by sulfate and oxalate or via cloud processing (Bondy et al., 2017). However, the limitations of this traditional analysis include an oversimplification of aerosol mixing state by assuming nitrate, non-sea salt sulfate, and oxalate are associated only with dust.

4.2 Size-Resolved Aerosol Mixing State from CCSEM/EDX

Using size-resolved chemical data of individual particles from CCSEM/EDX analysis, we assessed the extent of aging across the aerosol size distribution. The role of particle size is important as smaller dust particles have higher surface area-to-volume ratios that have been suggested to increase the propensity for dust aging (Baker & Jickells, 2006). Results from CCSEM/EDX analysis revealed the presence of both marine particles such as sea spray, aged sea spray, organics, and sulfates, as well as continental particle types including dust, internally mixed dust and sea salt, internally mixed dust and smoke from African wildfires, and externally mixed smoke from African wildfires that are described in detail in Royer et al., 2023. Here, we

focus on 4 particle types relevant to the understanding of dust aging during the sampling period: dust, sea spray (combined sea spray and aged sea spray), internally mixed dust and sea salt, and internally mixed dust and smoke.

Figure 2 presents detailed size-resolved chemical data for the four particle types of interest during periods of dust transport to Barbados, providing insight into the extent of particle aging across the aerosol size distribution. In Figure 2a, particle types are plotted as number fractions of the aerosol loading as a function of aerosol diameter. While dust mass concentrations from our filters for the submicron ($<1.3 \mu\text{m}$) and supermicron ($>1.3 \mu\text{m}$) aerosol loading are similar at $14.4 \mu\text{g}/\text{m}^3$ and $12.3 \mu\text{g}/\text{m}^3$, respectively, similar to results found for Asian dust (Zhang et al., 2023), CCSEM analysis reveals that dust only makes up 21% and 4% of the submicron ($<1 \mu\text{m}$) and supermicron ($1\text{--}5 \mu\text{m}$) aerosol loading by particle number, respectively. We note that part of this discrepancy could be because the CCSEM analysis is restricted to an upper limit of $5 \mu\text{m}$ in diameter. Figure 2a reveals that internal mixtures of dust with other components such as sea salt and smoke are, in fact, more abundant in the aerosol size distribution compared to dust alone, specifically in the supermicron aerosol loading. Internal mixtures of dust and sea salt comprise 11% of the submicron and 45% of the supermicron aerosol loading, while internal mixtures of dust and smoke comprise 14% of the submicron and 8% of the supermicron aerosol loading. These data reveal a complexity in the aerosol loading overlooked by bulk aerosol analysis, and call into question the assumption that the presence of nitrate, non-sea salt sulfate, and oxalate in bulk samples indicates aging of individual dust particles.

Figures 2b, c, d, and e present the average detectable nitrogen (N) content (left axis) and number fraction of N-containing particles (right axis) as a function of particle size for sea salt, internally mixed dust and sea salt, internally mixed dust and smoke, and dust particles,

respectively. Values for average N content and particle fractions with detectable N for each particle type are reported in the Supporting Information (SI) tables S1 and S2, respectively. Notably, average N content within individual particles is similar for all 4 particle types, ranging from $2.0 \pm 0.5\%$ to $2.6 \pm 0.4\%$ N with an average N content of $2.2 \pm 0.6\%$. However, between the 4 particle types, there are large variations in the number of particles containing detectable N, which is found in $36 \pm 25\%$ of submicron and $76 \pm 12\%$ of supermicron dust particles. This corroborates findings from bulk aerosol analysis which shows that nitrate is more concentrated in the supermicron aerosol loading compared to the submicron aerosol loading. However, Figure 2a reveals that dust only comprises 13% of the aerosol loading by number, with a much larger contribution in the submicron aerosol loading. Considering that individual particles containing detectable N on average have a N content of $2.2 \pm 0.6\%$, dust alone cannot explain trends in bulk nitrate. Figure 2c, d, and e all indicate the presence of N in particles aside from dust. Most notably, internally mixed dust and sea salt, which makes up 45% of the supermicron aerosol loading, has detectable N in $75 \pm 14\%$ of supermicron particles, potentially explaining the high supermicron nitrate content from bulk aerosol analysis.

Figures 2f, g, h, and i present the average detectable sulfur (S) content and number fraction of S-containing particles for the 4 particle types of interest. Values for average S content and particle fractions with detectable S for each particle type are reported in SI tables S3 and S4, respectively. Similarly to Figures 2b, c, d, and e, the S content in individual particles does not vary much across the aerosol size distribution for each particle type, with the average S content for the total aerosol loading ranging from $1.7 \pm 0.5\%$ to $2.7 \pm 0.5\%$ and averaging $2.4 \pm 1.2\%$. However, the number fractions of particles with detectable S do vary across the aerosol size distribution and between particle types. Only $8 \pm 7\%$ of submicron and $14 \pm 15\%$ of supermicron

dust particles contained detectable S, indicating a large discrepancy between dust particles containing S and the sulfate mass concentrations observed from our filter analysis. For almost all particle types across the aerosol size distribution, with the exception of supermicron internal mixtures of dust and smoke, S content exceeds that of dust. Internal mixtures of dust and sea salt far exceed the S content in dust with $28 \pm 9\%$ of submicron and $35 \pm 19\%$ of supermicron internally mixed dust and sea salt particles containing S. This is especially relevant as internal mixtures of dust and sea salt comprise a much larger portion of the supermicron aerosol loading at 45%, compared to dust at 4%. Sea salt particles, which also make up a much larger portion of the particle loading than dust at 55% of the submicron and 44% of the supermicron aerosol loading, also contained larger number fractions of particles with detectable S where $36 \pm 22\%$ of submicron and $87 \pm 58\%$ of supermicron sea salt particles had observable S. Observed S in sea salt and internal mixtures of dust and sea salt may explain the observed non-sea salt sulfate mass concentrations detected in the supermicron size range of our filter samples. However, an increase in S in sea salt particles across the size distribution is, in part, likely the result of calcium-sulfate minerals that often form on larger sea salt particles (Ault et al., 2013; Bondy et al., 2018; Choël et al., 2007). Despite the larger mass concentration of non-sea salt sulfate in the submicron size mode of our filters, number fractions of particles containing detectable S were greater in the supermicron size range compared to the submicron size range for all four particle types except internally mixed dust and smoke, which only comprises 14% of the submicron aerosol loading and has an average S content of $2.7 \pm 1.0\%$ for submicron particles. Instead, high mass concentrations of sulfate observed in submicron IC analysis are likely caused by ammonium sulfate particles observed during the sampling period. Previous studies show sulfate particles are primarily submicron in size and comprise a large fraction of the submicron aerosol loading

during both clean marine conditions and African dust transport (Rodriguez et al., 2011), which may contribute high non-sea salt sulfate mass detectable in bulk aerosol analysis but not in S content for the four particle types of interest (Royer et al., 2023).

Ternary plots presented in Figure 3 provide insight into the chemical mixing state of detected particles during the EUREC⁴A/ATOMIC campaign. Single particles are represented by individual dots in each ternary plot. The color of each dot indicates the diameter of the particle it represents. The position of each dot within the ternary plot indicates the relative abundance of sulfur (S, left vertex), chlorine (Cl, top vertex), and nitrogen (N, right vertex) within each particle. Sea salt particles displayed in Figure 3a are clustered primarily at the top vertex indicating high Cl content, low S content, and low N content characteristic of freshly emitted sea salt. Particle clustering at the left and right vertices demonstrates aging of sea salt particles as low Cl content and high S and/or N content suggests chloride has been depleted and replaced with nitrate and sulfate during heterogeneous reactions (Ault et al., 2013, 2014; Behnke et al., 1997; Gaston et al., 2011, 2013; Sobanska et al., 2003). Differences in color at each vertex within Figure 3a also indicates that aged sea salt particles are smaller than fresh sea salt particles on average (Laskin et al., 2012).

Dust and internally mixed dust and smoke particles are primarily in the submicron size range, as indicated in Figure 2, and cluster at the right vertex indicating the presence of more N compared to S and Cl in these particles, but these particles are sparse in number concentration. Internally mixed dust and sea salt particles cluster primarily along the right axis of the ternary plot, exhibiting various levels of Cl likely from sea salt, low S, and varying N content. Notably, larger particles identified as internally mixed dust and sea salt had elevated chloride compared to S and N while smaller particles had less chloride and elevated S and N. Figure 3 demonstrates

that, of the particle types containing dust components, internal mixtures of dust and sea salt are the most abundant in the aerosol loading and had the highest number of aged particles containing detectable N and S. As such, we focus our subsequent analysis of chemical aging on internally mixed dust and sea salt.

4.3 Elemental Mapping and EDX Analysis to Determine Spatial Patterns of Chemical Aging Markers on Individual Particles

While analysis by CCSEM/EDX is valuable for determining size-resolved aerosol mixing state, this method does not map the distribution of elements within each particle, which leads to uncertainty regarding the location of the aging components within the particles, particularly for internally mixed particle types. The elemental mapping image depicted in Figure 4a shows the distribution of elements across an entire particle. The presence of distinct areas of dust components such as Si, Al, Ca, Fe, and Mg that are separate from sea salt components such as Na and Cl within a single particle indicates that the particle is a typical internally mixed dust and sea salt particle. Within the image, the distribution of nitrogen and sulfur are depicted as well, and visually appear present only over the sea salt components. Spectra from EDX analysis were extracted from these distinct regions on the particle which reveal that nitrogen and sulfur are indeed either negligible or completely absent on the dust components ($S = 0.1\%$; $N = 0\%$), while they are present in appreciable quantities on the sea salt components ($S = 2.9\%$; $N = 2.9\%$). Also worth noting is the absence of Cl in the sea salt component, which is indicative of sea salt aging also observed in CCSEM/EDX analysis. This particle is representative of internally mixed dust and sea salt particles detected during the sampling period that similarly show only aging on the sea salt components. Additional examples of internally mixed dust and sea salt particle elemental maps and EDX spectra are provided in Figure S3 of the SI. In addition, elemental maps and

corresponding EDX spectra for dust, sea salt, smoke, and internally mixed dust and smoke are provided in Figure S4. Similar to the internally mixed dust and sea spray particles, externally mixed dust and the dust component that is internally mixed with smoke show a lack of aging while the smoke components in mixed dust and smoke particles show extensive accumulation of sulfur. These results suggest that even in internal mixtures of dust, only the sea salt (or smoke) components are undergoing aging at least with S while dust shows a lack of chemical aging markers.

4.4 TOF-SIMS Imaging of Chemical Markers of Aerosol Aging

Results from TOF-SIMS analysis corroborate findings from SEM/EDX elemental mapping, indicating that aging of internally mixed dust and sea salt particles occurs primarily on the sea salt components. Figure 5 depicts results from TOF-SIMS imaging in which the color intensity in each image represents the intensity of an ion. The cation images in the top panel indicate the presence of sea salt (Na_2Cl^+) and dust (Al^+ and Ca^+), while the last cation image on the righthand side shows all ions plotted together. The cation image indicates that while the majority of the particles in the image presented are sea salt particles due to the abundance of Na_2Cl^+ , the co-location of sea salt components with dust components Al^+ and Ca^+ suggest there is internal mixing of dust and sea salt as well. The anion images in the bottom panel similarly plot individual ions, with the anions indicating the presence of sea salt (NaCl_2^-) and chemical markers of aging from sulfate and nitrate (HSO_4^- and NO_3^- , respectively) as well as a final image containing all anions plotted together. Once again, the presence of the anion NaCl_2^- suggests that sea salt is abundant and further corroborates the cation images. The presence of HSO_4^- and NO_3^- provide insight into the extent of aging on the particles presented in the images which show a strong presence of aging from sulfate through the presence of HSO_4^- but a lack of aging from

nitrate through the absence of NO_3^- . Most notably, in the image overlaying all anions together, the NaCl_2^- and HSO_4^- are indistinguishable from one another, indicating aging on the sea salt components. Comparing the cation image to the anion image, it is clear that the areas in which dust components are present are not undergoing aging, rather, primarily the sea salt components are being aged. This supports findings from elemental mapping from SEM/EDX analysis which similarly suggest minimal aging of dust components but aging of sea spray components in these internally mixed particles.

Discussion & Conclusion

Traditional methods for studying dust aging often measure dust concentrations (or their proxies) and soluble materials extracted from aerosol filters have historically used correlations between nss-sulfate, oxalate, and nitrate and dust mass concentrations to prove the presence of dust aging. However, these methods have been unable to determine the mixing state of dust and, thus, whether dust (or another aerosol type) is actually undergoing chemical aging (Chen & Siefert, 2004; Li-Jones & Prospero, 1998). The results from this work indicate that while internal mixtures of dust with other particles are common in the lower boundary layer, both internally and externally mixed African dust detected in the western Atlantic are minimally aged during the wintertime. The boreal winter provides the most ideal conditions for African dust chemical aging to occur due to the lower transport altitude creating more time for MBL emissions to interact with long range transported dust. Further, wintertime dust is often co-transported with Sahelian biomass burning and industrial emissions contributing high concentrations of NO_x and SO_2 that are co-transported with dust, allowing for interaction of dust with gases that can induce chemical aging over several days during transatlantic transport (Hickman et al., 2021). The lack of aging on internal mixtures of dust and smoke indicate rapid conversion of NO_x and SO_2 to nitrate and

sulfate on smoke, which is corroborated by the presence of potassium sulfate salts observed on smoke particles from EUREC⁴A/ATOMIC and a lack of these compounds on dust (Royer et al., 2023). The lack of dust aging indicators observed during the winter may indicate a lack of aging throughout the year for long range transported African dust. This is apparent from size-resolved CCSEM/EDX data which indicate a lack of aging on dust particles by sulfate and nitrate, and from elemental mapping and TOF-SIMS imaging which show that chemical aging is favored on the sea spray and smoke components of internally mixed dust particles. Our findings of aged sea spray, with losses of chloride, on internally mixed dust and sea spray particles could also indicate an increase in the heterogeneous displacement of chloride from these internally mixed particles compared to sea spray alone (van Herpen et al., 2023).

It is likely that dust is being aged in the eastern Atlantic, but is removed during long range transport to the western Atlantic based on previous studies (Abdelkader et al., 2017). The lower altitude for dust transport during the wintertime would also provide ample opportunity for dust aging in the eastern Atlantic which could lead to the rapid aging of dust particles before long range transport (Chiapello et al., 1995; Kandler et al., 2011; Ullerstam et al., 2002). The addition of high levels of pollutants from North African industrial emissions and the Sahelian fires could also exacerbate aging in the eastern Atlantic (Andreae et al., 2000; Rodriguez et al., 2011). Aged dust particles are much more efficiently removed by both wet and dry deposition as well as cloud droplet activation as a result of increased water uptake properties enhancing their size and reactivity (Abdelkader et al., 2017; Gaston, 2020; Metzger et al., 2006). It is possible that the rapid aging of dust particles in the eastern Atlantic upon dust emission increases the water uptake properties of the dust, leading to rapid removal of dust particles before long range transport can carry dust particles to the western Atlantic. This potentially explains the minimal

aging of dust particles in the western Atlantic, as any aged dust is likely removed before arriving over Barbados.

Based on the high abundance of internally mixed dust and sea salt particles in the aerosol loading, it is likely that unaged dust transported across the Atlantic becomes associated with aged sea spray as dust is being detrained from the SAL into the MBL as suggested in previous studies (Abdelkader et al., 2017). This would result in altitudinal gradients in dust mixing state important for dust radiative impacts. Though dust components in the lower boundary layer are rarely aged, internal mixtures of dust with other components such as sea salt and smoke are common. The high degree of aging on these internally mixed components suggest internal dust mixtures are more hygroscopic and, thus, are potentially efficient as cloud condensation nuclei.

The lack of aging on dust components has implications for nutrient availability in mineral dust aerosols transported to the tropical Atlantic as well. Ecosystems in the tropical Atlantic such as the open Atlantic Ocean and the Amazon rainforest rely on external inputs of nutrients such as iron and phosphorus (Fe and P). Chemical aging is particularly important to provide bioavailable sources of nutrients to marine ecosystems, as deposition of particles out of the euphotic zone competes with nutrient release into seawater (Gaston, 2020). The lack of chemical aging on mineral dust observed in this study suggests that the chemical aging of dust plays a limited role in observed increases in nutrient solubility during transatlantic transport, consistent with findings for Asian dust (Chen et al, 2024).

In this work, we utilized methods that target aerosol mixing state to determine the extent of aging in long range transported African dust particles to the western Atlantic during the wintertime. The disparity between bulk methods, which suggest dust aging is extensive, and methods that characterize the aerosol mixing state, which reveal a distinct lack of aging for dust

components, reveals the importance of utilizing single-particle methods to understand dust aging (Fitzgerald et al., 2015; Kandler et al., 2011). We also provide much-needed insight into the question of dust aging in the western Atlantic, revealing limited aging for dust particles in the wintertime that should be considered in global and regional models.

Data Availability

Dust and soluble ion mass concentration data and number counts of particle types detected by CCSEM/EDX will be publicly available in the University of Miami data repository.

Author Contribution:

Conceptualization of this work was performed by HMR, APA, and CJG. Collection of samples was conducted by HMR and EB, while analysis was done by HMR, MS, HE, NNL, ZC, and ZZ. Development of methods used in this work was done by HMR, ZC, SC, APA, and CJG. Instrumentation used to conduct this work was provided by CJG, APA, SC, and ZZ. Validation of data products was performed by HMR, ZC, APA, and CJG. Computer code used for data analysis was provided by APA. Data visualization was performed by HMR, APA, and CJG. Supervision and project administration duties were conducted by CJG. CJG is responsible for funding acquisition. HMR wrote the original draft for publication, and all co-authors reviewed and edited this work.

Competing Interests: The authors declare that they have no conflict of interest.

Acknowledgements

C.J.G. acknowledges an NSF CAREER award (1944958). A portion of this research was performed on project awards (10.46936/lser.proj.2019.50816/60000110 and 10.46936/lser.proj.2021.51900/60000361) from the Environmental Molecular Sciences

Laboratory, a DOE Office of Science User Facility sponsored by the Biological and Environmental Research program under Contract No. DE-AC05-76RL01830.

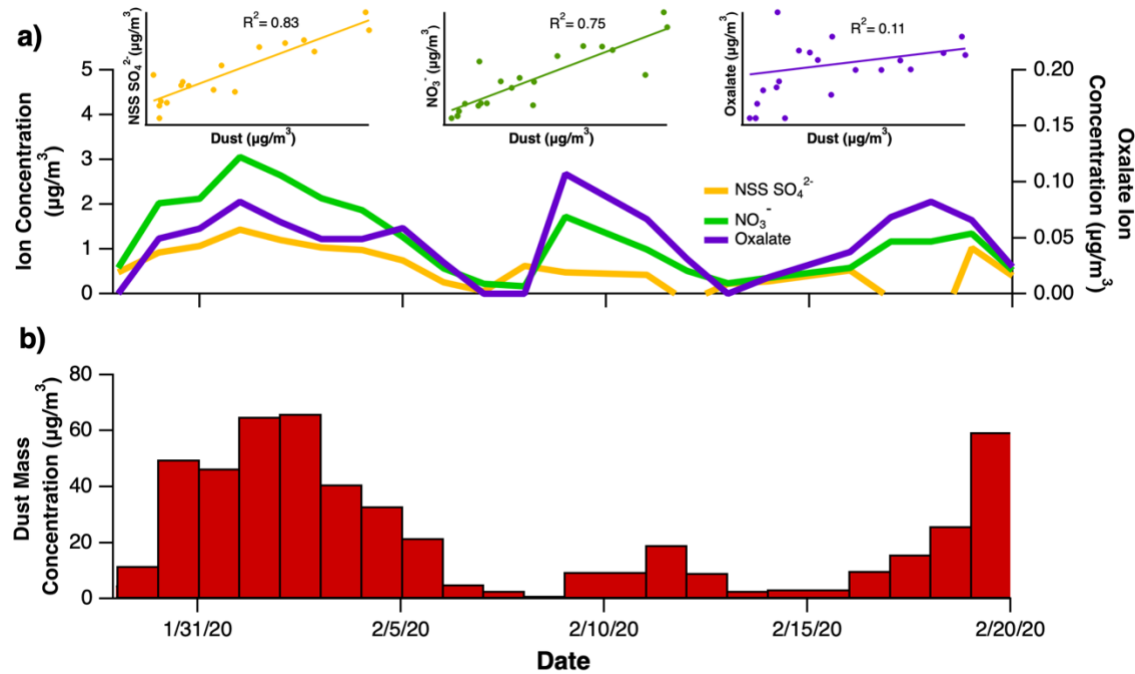


Figure 1 – a) Daily bulk soluble ion content for nitrate (left axis; green line), non-sea salt sulfate (left axis; yellow line), and oxalate (right axis; purple line) with correlation plots for each ion as a function of dust mass concentrations and b) daily bulk dust mass concentrations determined for the entire sampling period. Correlation plots include all data, including data from samples with undetectable ions, but trendlines only consider data with detectable dust and ions.

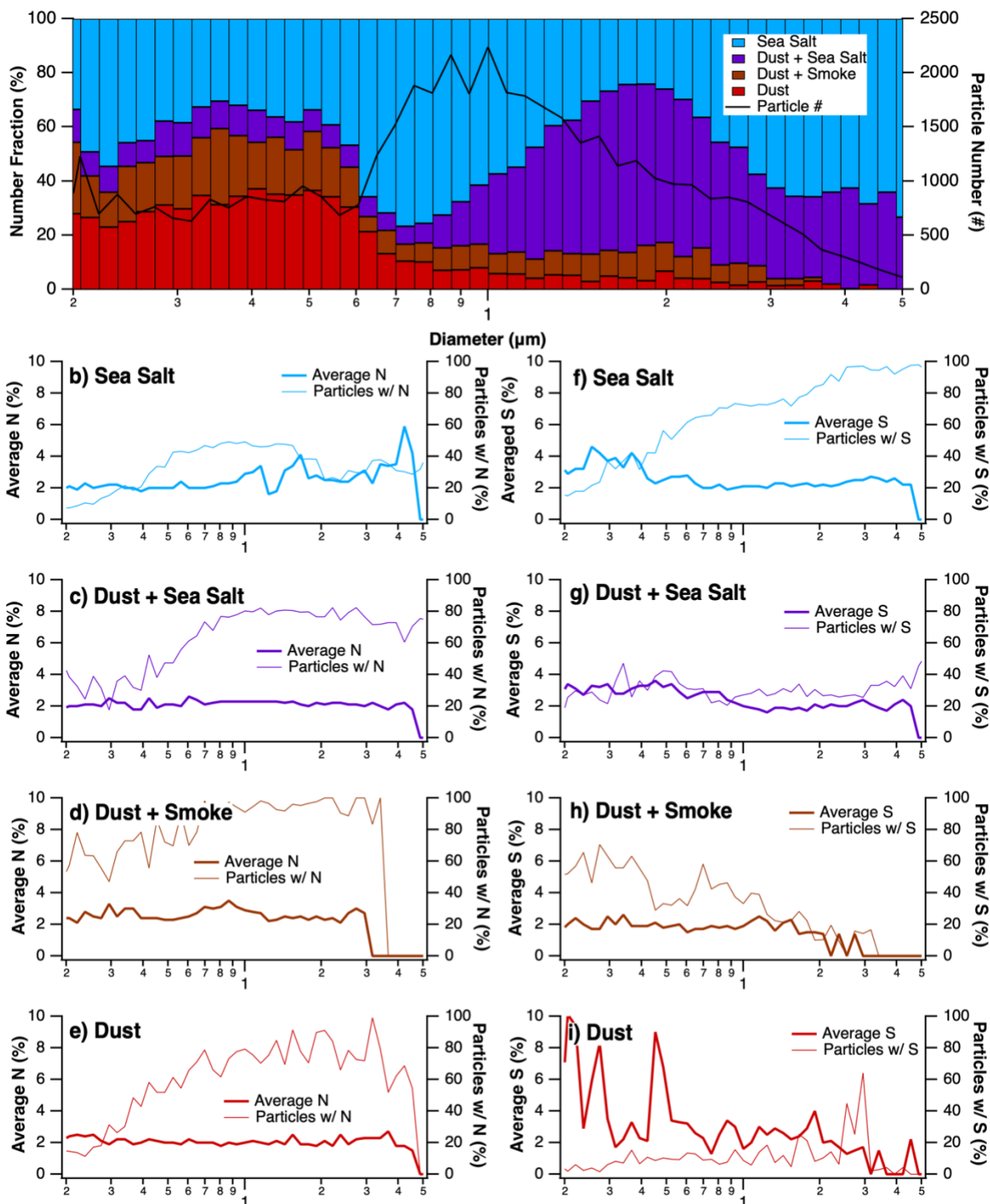
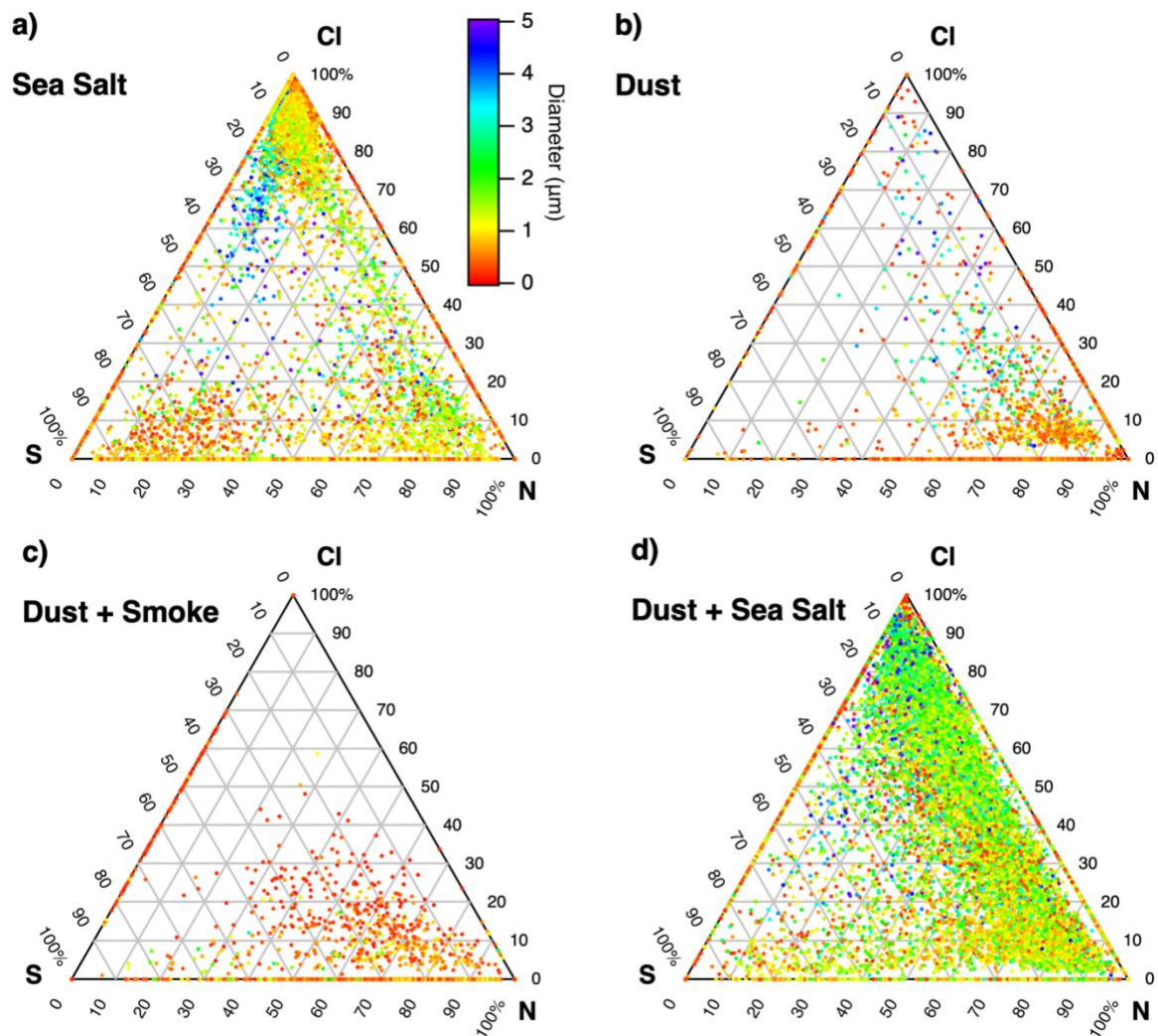


Figure 2 – Size-resolved chemistry plots summarized by a) a total size-resolved chemistry plot in which the particle number loading is normalized to the sum of sea salt particles (blue), internally mixed dust and sea salt particles (purple), internally mixed dust and smoke particles (brown), and

568 dust particles (red) for each size bin and presented as a fraction of the particle number loading in
569 each size bin (left axis) along with the total sum of the number of particles of interest for each
570 size bin (right axis: black line). Plots depicting the average nitrogen (N) or sulfur (S) content in
571 individual particles (left axis; thick line) as well as the number fraction of particles in each size
572 bin containing nitrogen or sulfur (right axis; thin line) are provided for b) nitrogen in sea salt
573 particles, c) nitrogen in internally mixed dust and sea salt particles, d) nitrogen in internally
574 mixed dust and smoke particles, e) nitrogen in dust particles, f) sulfur in sea salt particles, g)
575 sulfur in internally mixed dust and sea salt particles, h) sulfur in internally mixed dust and smoke
576 particles, and i) sulfur in dust particles.



577
 578 Figure 3 – Ternary plots presenting the normalized percentage of sulfur (S) (left axis), chlorine
 579 (Cl), (right axis), and nitrogen (N) (bottom axis) present in dust (6,426 particles), internally
 580 mixed dust + smoke (1,588 particles), internally mixed dust + sea salt (18,210 particles), and sea
 581 salt (22,354 particles). Color scaling denotes particle diameter.

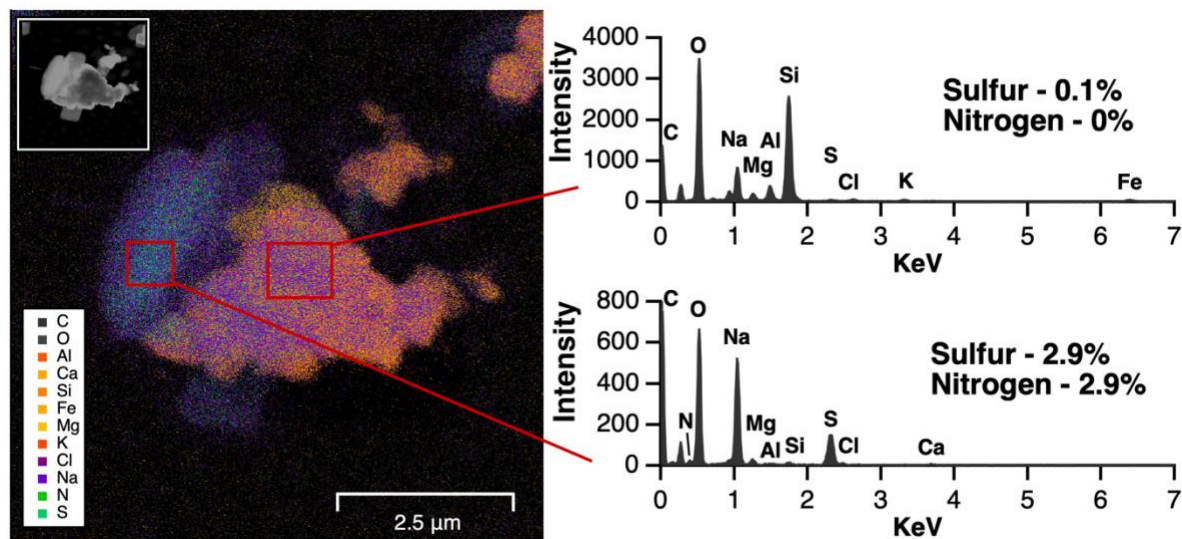


Figure 4 – Elemental mapping image from SEM/EDX analysis for an internally mixed dust and sea salt particle collected at Ragged Point on 2/9/2020 on stage 2 of the MPS. Top left plot depicts the SEM image. The legend explains the color associated with each element plotted in the elemental map with warm colors denoting dust components, cool colors denoting sea spray components and green colors denoting aging markers. Red squares on the elemental map indicate where EDX spectra were extracted for the dust component, which is shown in the top right plot, and the sea salt component, shown in the bottom right plot, of the particle. Sulfur and nitrogen values represent calculated EDX intensity present on dust and sea spray components of the particle.

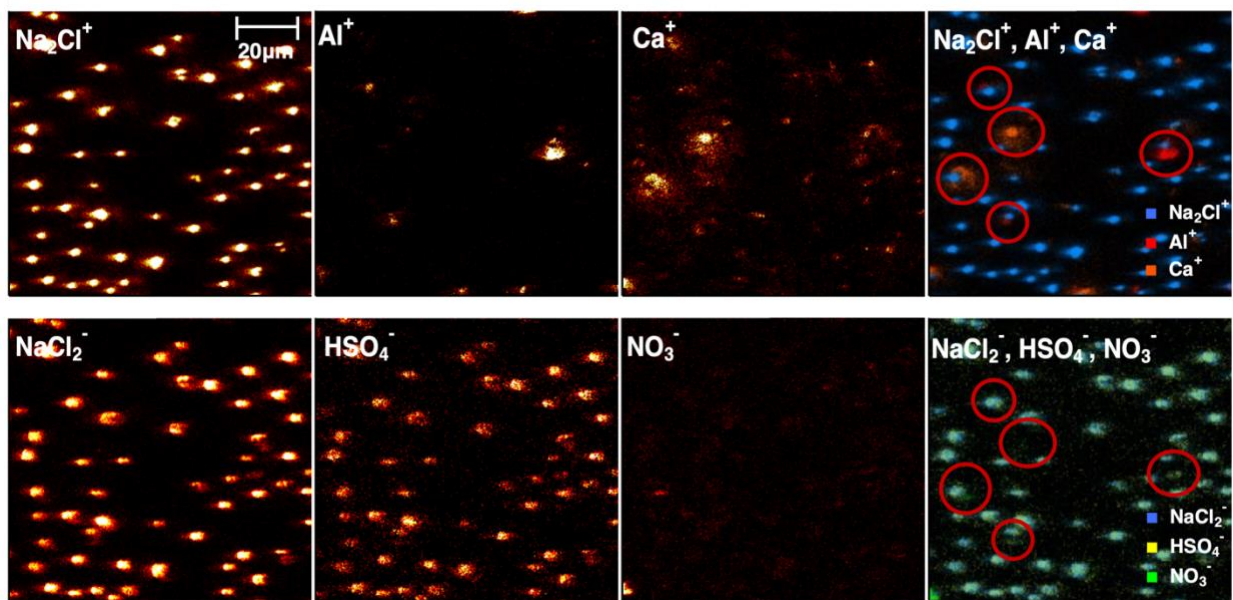


Figure 5 – Image plots from TOF-SIMS analysis of a sample collected on 2/18/2020 from stage 1 of the MPS. Red circles mark the location of dust components of the particles. The top panel shows images of cations indicative of sea salt (Na_2Cl^+), dust (Al^+ and Ca^+), and a combined plot showing all three markers. The bottom panel shows anions indicative of sea salt (NaCl_2^-), chemical aging markers (sulfate (HSO_4^-), nitrate (NO_3^-)) and a combined plot showing all three markers.

References

- Abdelkader, M., Metzger, S., Mamouri, R. E., Astitha, M., Barrie, L., Levin, Z., & Lelieveld, J. (2015). Dust–air pollution dynamics over the eastern Mediterranean. *Atmospheric Chemistry and Physics*, 15(16), 9173–9189. <https://doi.org/10.5194/acp-15-9173-2015>
- Abdelkader, M., Metzger, S., Steil, B., Klingmüller, K., Tost, H., Pozzer, A., Stenchikov, G., Barrie, L., & Lelieveld, J. (2017). Sensitivity of transatlantic dust transport to chemical aging and related atmospheric processes. *Atmospheric Chemistry and Physics*, 17(6), 3799–3821. <https://doi.org/10.5194/acp-17-3799-2017>
- Albrecht, B. A. (1989). Aerosols, cloud microphysics, and fractional cloudiness. *Science*, 245(4923), 1227–1230. <https://doi.org/10.1126/science.245.4923.1227>
- Andreae, M O, Elbert, W., Gabriel, R., Johnson, D. W., Osborne, S., & Wood, R. (2000). Soluble ion chemistry of the atmospheric aerosol and SO₂ concentrations over the eastern North Atlantic during ACE-2. *Tellus B: Chemical and Physical Meteorology*. <https://doi.org/10.3402/tellusb.v52i4.17087>
- Andreae, Meinrat O. (1983). Soot Carbon and Excess Fine Potassium: Long-Range Transport of Combustion-Derived Aerosols. *Science*, 220(4602), 1148–1151. <https://doi.org/10.1126/science.220.4602.1148>
- Andreae, Meinrat O, Charlson, R. J., Bruynseels, F., Storms, H., Grieken, R. Van, & Maenhaut, W. (1986). Internal Mixture of Sea Salt, Silicates, and Excess Sulfate in Marine Aerosols. *Science*, 232(4758), 1620–1623. <https://doi.org/10.1126/science.232.4758.1620>
- Archibald, A. T., Witham, C. S., Ashfold, M. J., Manning, A. J., O’Doherty, S., Grealley, B. R., Young, D., & Shallcross, D. E. (2015). Long-term high frequency measurements of ethane, benzene and methyl chloride at Ragged Point, Barbados: Identification of long-range transport events. *Elementa: Science of the Anthropocene*, 3. <https://doi.org/10.12952/journal.elementa.000068>
- Archuleta, C. M., DeMott, P. J., & Kreidenweis, S. M. (2005). Ice nucleation by surrogates for atmospheric mineral dust and mineral dust/sulfate particles at cirrus temperatures. *Atmospheric Chemistry and Physics*, 5(10), 2617–2634. <https://doi.org/10.5194/acp-5-2617-2005>
- Ault, A. P., Peters, T. M., Sawvel, E. J., Casuccio, G. S., Willis, R. D., Norris, G. A., & Grassian, V. H. (2012). Single-Particle SEM-EDX Analysis of Iron-Containing Coarse Particulate Matter in an Urban Environment: Sources and Distribution of Iron within Cleveland, Ohio. *Environmental Science & Technology*, 46(8), 4331–4339. <https://doi.org/10.1021/es204006k>
- Ault, A. P., Moffet, R. C., Baltrusaitis, J., Collins, D. B., Ruppel, M. J., Cuadra-Rodriguez, L. A., Zhao, D., Guasco, T. L., Ebben, C. J., Geiger, F. M., Bertram, T. H., Prather, K. A., & Grassian, V. H. (2013). Size-Dependent Changes in Sea Spray Aerosol Composition and Properties with Different Seawater Conditions. *Environmental Science & Technology*, 47(11), 5603–5612. <https://doi.org/10.1021/es400416g>
- Ault, A. P., Guasco, T. L., Baltrusaitis, J., Ryder, O. S., Trueblood, J. V., Collins, D. B., Ruppel, M. J., Cuadra-Rodriguez, L. A., Prather, K. A., & Grassian, V. H. (2014). Heterogeneous Reactivity of Nitric Acid with Nascent Sea Spray Aerosol: Large Differences Observed between and within Individual Particles. *The Journal of Physical Chemistry Letters*, 5(15), 2493–2500. <https://doi.org/10.1021/jz5008802>
- Baker, A. R., & Jickells, T. D. (2006). Mineral particle size as a control on aerosol iron

- solubility. *Geophysical Research Letters*, 33(17), 1–4.
<https://doi.org/10.1029/2006GL026557>
- Balkanski, Y., Schulz, M., Claquin, T., & Guibert, S. (2007). Reevaluation of Mineral aerosol radiative forcings suggests a better agreement with satellite and AERONET data. *Atmospheric Chemistry and Physics*, 7(1), 81–95. <https://doi.org/10.5194/acp-7-81-2007>
- Barkley, A. E., Prospero, J. M., Mahowald, N., Hamilton, D. S., Popendorf, K. J., Oehlert, A. M., Pourmand, A., Gatineau, A., Panechou-Pulcherie, K., Blackwelder, P., & Gaston, C. J. (2019). African biomass burning is a substantial source of phosphorus deposition to the Amazon, Tropical Atlantic Ocean, and Southern Ocean. *Proceedings of the National Academy of Sciences*, 116(33), 16216 LP – 16221. <https://doi.org/10.1073/pnas.1906091116>
- Bauer, S. E., Mishchenko, M. I., Lacis, A. A., Zhang, S., Perlwitz, J., & Metzger, S. M. (2007). Do sulfate and nitrate coatings on mineral dust have important effects on radiative properties and climate modeling? *Journal of Geophysical Research: Atmospheres*, 112(D6). <https://doi.org/10.1029/2005JD006977>
- Behnke, W., George, C., Scheer, V., & Zetzsch, C. (1997). Production and decay of ClNO₂ from the reaction of gaseous N₂O₅ with NaCl solution: Bulk and aerosol experiments. *Journal of Geophysical Research Atmospheres*, 102(3), 3795–3804. <https://doi.org/10.1029/96jd03057>
- Bondy, A L, Bonanno, D., Moffet, R. C., Wang, B., Laskin, A., & Ault, A. P. (2018). The diverse chemical mixing state of aerosol particles in the southeastern United States. *Atmospheric Chemistry and Physics*, 18(16), 12595–12612. <https://doi.org/10.5194/acp-18-12595-2018>
- Bondy, Amy L, Wang, B., Laskin, A., Craig, R. L., Nhliziyo, M. V, Bertman, S. B., Pratt, K. A., Shepson, P. B., & Ault, A. P. (2017). Inland Sea Spray Aerosol Transport and Incomplete Chloride Depletion: Varying Degrees of Reactive Processing Observed during SOAS. *Environmental Science & Technology*, 51(17), 9533–9542. <https://doi.org/10.1021/acs.est.7b02085>
- Carlson, T. N., & Prospero, J. M. (1972). The Large-Scale Movement of Saharan Air Outbreaks over the Northern Equatorial Atlantic. *Journal of Applied Meteorology and Climatology*, 11(2), 283–297. [https://doi.org/10.1175/1520-0450\(1972\)011<0283:TLSMOS>2.0.CO;2](https://doi.org/10.1175/1520-0450(1972)011<0283:TLSMOS>2.0.CO;2)
- Chen, Y., & Siefert, R. L. (2004). Seasonal and spatial distributions and dry deposition fluxes of atmospheric total and labile iron over the tropical and subtropical North Atlantic Ocean. *Journal of Geophysical Research: Atmospheres*, 109(D9). <https://doi.org/10.1029/2003JD003958>
- Chen, Y.Z., Wang, Z.Y., Fang, Z.Y., Huang, C.P., Xu, H., Zhang, H.H., Zhang, T.Y., Wang, F., Luo, L., Shi, G.L., Wang, X.M., & Tang, M.J. (2024) Dominant contribution of non-dust primary emissions and secondary processes to dissolved aerosol iron. *Environmental Science & Technology*, 58, 17355-17363.
- Chiapello, I., Bergametti, G., Gomes, L., Chatenet, B., Dulac, F., Pimenta, J., & Soares, E. S. (1995). An additional low layer transport of Sahelian and Saharan dust over the north-eastern Tropical Atlantic. *Geophysical Research Letters*, 22(23), 3191–3194. <https://doi.org/10.1029/95GL03313>
- Choël, M., Deboudt, K., Flament, P., Aimo, L., & Mériaux, X. (2007). Single-particle analysis of atmospheric aerosols at Cape Gris-Nez, English Channel: Influence of steel works on iron apportionment. *Atmospheric Environment*, 41(13), 2820–2830. <https://doi.org/10.1016/j.atmosenv.2006.11.038>
- Cziczo, D. J., Murphy, D. M., Hudson, P. K., & Thomson, D. S. (2004). Single particle

- measurements of the chemical composition of cirrus ice residue during CRYSTAL-FACE. *Journal of Geophysical Research: Atmospheres*, 109(D4).
<https://doi.org/https://doi.org/10.1029/2003JD004032>
- DeMott, P. J., Sassen, K., Poellot, M. R., Baumgardner, D., Rogers, D. C., Brooks, S. D., Prenni, A. J., & Kreidenweis, S. M. (2003). African dust aerosols as atmospheric ice nuclei. *Geophysical Research Letters*, 30(14).
<https://doi.org/https://doi.org/10.1029/2003GL017410>
- Denjean, C., Caquineau, S., Desboeufs, K., Laurent, B., Maille, M., Quiñones Rosado, M., Vallejo, P., Mayol-Bracero, O. L., & Formenti, P. (2015). Long-range transport across the Atlantic in summertime does not enhance the hygroscopicity of African mineral dust. *Geophysical Research Letters*, 42(18), 7835–7843.
<https://doi.org/https://doi.org/10.1002/2015GL065693>
- Desboeufs, K., Formenti, P., Torres-Sánchez, R., Schepanski, K., Chaboureaud, J.-P., Andersen, H., Cermak, J., Feuerstein, S., Laurent, B., Klopfer, D., Namwoonde, A., Cazaunau, M., Chevaillier, S., Feron, A., Mirande-Bret, C., Triquet, S., & Piketh, S. J. (2024). Fractional solubility of iron in mineral dust aerosols over coastal Namibia: a link to marine biogenic emissions? *Atmospheric Chemistry and Physics*, 24(2), 1525–1541.
<https://doi.org/10.5194/acp-24-1525-2024>
- Elliott, H. E., Pependorf, K. J., Blades, E., Royer, H. M., Pollier, C. G. L., Oehlert, A. M., Kukkadapu, R., Ault, A., & Gaston, C. J. (2024). Godzilla mineral dust and La Soufrière volcanic ash fallout immediately stimulate marine microbial phosphate uptake, 10.
<https://doi.org/https://doi.org/10.3389/fmars.2023.1308689>
- Fitzgerald, E., Ault, A. P., Zauscher, M. D., Mayol-Bracero, O. L., & Prather, K. A. (2015). Comparison of the mixing state of long-range transported Asian and African mineral dust. *Atmospheric Environment*, 115, 19–25.
<https://doi.org/https://doi.org/10.1016/j.atmosenv.2015.04.031>
- Gaston, C. J. (2020). Re-examining Dust Chemical Aging and Its Impacts on Earth’s Climate. *Accounts of Chemical Research*, 53(5), 1005–1013.
<https://doi.org/10.1021/acs.accounts.0c00102>
- Gaston, C. J., Pratt, K. A., Qin, X., & Prather, K. A. (2010). Real-time detection and mixing state of methanesulfonate in single particles at an inland urban location during a phytoplankton bloom. *Environmental Science and Technology*, 44(5), 1566–1572.
<https://doi.org/10.1021/es902069d>
- Gaston, C. J., Furutani, H., Guazzotti, S. A., Coffee, K. R., Bates, T. S., Quinn, P. K., Aluwihare, L. I., Mitchell, B. G., & Prather, K. A. (2011). Unique ocean-derived particles serve as a proxy for changes in ocean chemistry. *Journal of Geophysical Research Atmospheres*, 116(18), 1–13. <https://doi.org/10.1029/2010JD015289>
- Gaston, C. J., Quinn, P. K., Bates, T. S., Gilman, J. B., Bon, D. M., Kuster, W. C., & Prather, K. A. (2013). The impact of shipping, agricultural, and urban emissions on single particle chemistry observed aboard the R/V Atlantis during CalNex. *Journal of Geophysical Research Atmospheres*, 118(10), 5003–5017. <https://doi.org/10.1002/jgrd.50427>
- Gaston, C.J., Prospero, J.M., Foley, K., Pye, H.O.T., Custals, L., Blades, E., Sealy, P., & Christie, J.A. (2024) Diverging trends in aerosol sulfate and nitrate measured in the remote North Atlantic on Barbados are attributed to clean air policies, African smoke, and anthropogenic emissions. *Atmospheric Chemistry & Physics*, 24(13), 8049–8066.
- Gibson, E. R., Gierlus, K. M., Hudson, P. K., & Grassian, V. H. (2007). Generation of Internally

- Mixed Insoluble and Soluble Aerosol Particles to Investigate the Impact of Atmospheric Aging and Heterogeneous Processing on the CCN Activity of Mineral Dust Aerosol. *Aerosol Science and Technology*, 41(10), 914–924. <https://doi.org/10.1080/02786820701557222>
- Gierlus, K. M., Laskina, O., Abernathy, T. L., & Grassian, V. H. (2012). Laboratory study of the effect of oxalic acid on the cloud condensation nuclei activity of mineral dust aerosol. *Atmospheric Environment*, 46, 125–130. <https://doi.org/https://doi.org/10.1016/j.atmosenv.2011.10.027>
- Gutleben, M., Groß, S., Heske, C., & Wirth, M. (2022). Wintertime Saharan dust transport towards the Caribbean: an airborne lidar case study during EUREC⁴A. *Atmospheric Chemistry and Physics*, 22(11), 7319–7330. <https://doi.org/10.5194/acp-22-7319-2022>
- Han, X., Zhang, M., Han, Z., Xin, J., & Liu, X. (2011). Simulation of aerosol direct radiative forcing with RAMS-CMAQ in East Asia. *Atmospheric Environment*, 45(36), 6576–6592. <https://doi.org/https://doi.org/10.1016/j.atmosenv.2011.08.006>
- Hand, V. L., Capes, G., Vaughan, D. J., Formenti, P., Haywood, J. M., & Coe, H. (2010). Evidence of internal mixing of African dust and biomass burning particles by individual particle analysis using electron beam techniques. *Journal of Geophysical Research: Atmospheres*, 115(D13). <https://doi.org/https://doi.org/10.1029/2009JD012938>
- Haywood, J., Francis, P., Osborne, S., Glew, M., Loeb, N., Highwood, E., Tanré, D., Myhre, G., Formenti, P., & Hirst, E. (2003). Radiative properties and direct radiative effect of Saharan dust measured by the C-130 aircraft during SHADE: 1. Solar spectrum. *Journal of Geophysical Research: Atmospheres*, 108(D18). <https://doi.org/https://doi.org/10.1029/2002JD002687>
- Hickman, J. E., Andela, N., Tsigaridis, K., Galy-Lacaux, C., Ossohou, M., & Bauer, S. E. (2021). Reductions in NO₂ burden over north equatorial Africa from decline in biomass burning in spite of growing fossil fuel use, 2005 to 2017. *Proceedings of the National Academy of Sciences*, 118(7), e2002579118. <https://doi.org/10.1073/pnas.2002579118>
- Hopkins, R. J., Desyaterik, Y., Tivanski, A. V., Zaveri, R. A., Berkowitz, C. M., Tylliszczak, T., Gilles, M. K., & Laskin, A. (2008). Chemical speciation of sulfur in marine cloud droplets and particles: Analysis of individual particles from the marine boundary layer over the California current. *Journal of Geophysical Research: Atmospheres*, 113(D4). <https://doi.org/https://doi.org/10.1029/2007JD008954>
- Jickells, T. D., An, Z. S., Andersen, K. K., Baker, A. R., Bergametti, G., Brooks, N., Cao, J. J., Boyd, P. W., Duce, R. A., Hunter, K. A., Kawahata, H., Kubilay, N., laRoche, J., Liss, P. S., Mahowald, N., Prospero, J. M., Ridgwell, A. J., Tegen, I., & Torres, R. (2005). Global Iron Connections Between Desert Dust, Ocean Biogeochemistry, and Climate. *Science*, 308(5718), 67–71. <https://doi.org/10.1126/science.1105959>
- Kandler, K., Lieke, K., Benker, N., Emmel, C., Küpper, M., Müller-Ebert, D., Ebert, M., Scheuvs, D., Schladitz, A., Schütz, L., & Weinbruch, S. (2011). Electron microscopy of particles collected at Praia, Cape Verde, during the Saharan Mineral Dust Experiment: particle chemistry, shape, mixing state and complex refractive index. *Tellus B: Chemical and Physical Meteorology*, 63(4), 475–496. <https://doi.org/10.1111/j.1600-0889.2011.00550.x>
- Kandler, K., Schneiders, K., Ebert, M., Hartmann, M., Weinbruch, S., Prass, M., & Pöhlker, C. (2018). Composition and mixing state of atmospheric aerosols determined by electron microscopy: method development and application to aged Saharan dust deposition in the

- Caribbean boundary layer. *Atmos. Chem. Phys.*, 18(18), 13429–13455.
<https://doi.org/10.5194/acp-18-13429-2018>
- Kelly, J. T., Chuang, C. C., & Wexler, A. S. (2007). Influence of dust composition on cloud droplet formation. *Atmospheric Environment*, 41(14), 2904–2916.
<https://doi.org/10.1016/j.atmosenv.2006.12.008>
- Koehler, K. A., Kreidenweis, S. M., DeMott, P. J., Petters, M. D., Prenni, A. J., & Carrico, C. M. (2009). Hygroscopicity and cloud droplet activation of mineral dust aerosol. *Geophysical Research Letters*, 36(8). <https://doi.org/10.1029/2009GL037348>
- Krueger, B. J., Grassian, V. H., Laskin, A., & Cowin, J. P. (2003). The transformation of solid atmospheric particles into liquid droplets through heterogeneous chemistry: Laboratory insights into the processing of calcium containing mineral dust aerosol in the troposphere. *Geophysical Research Letters*, 30(3). <https://doi.org/10.1029/2002GL016563>
- Krueger, B. J., Grassian, V. H., Cowin, J. P., & Laskin, A. (2004). Heterogeneous chemistry of individual mineral dust particles from different dust source regions: The importance of particle mineralogy. *Atmospheric Environment*, 38(36), 6253–6261.
<https://doi.org/10.1016/j.atmosenv.2004.07.010>
- Lance, S., Raatikainen, T., Onasch, T. B., Worsnop, D. R., Yu, X.-Y., Alexander, M. L., Stolzenburg, M. R., McMurry, P. H., Smith, J. N., & Nenes, A. (2013). Aerosol mixing state, hygroscopic growth and cloud activation efficiency during MIRAGE 2006. *Atmospheric Chemistry and Physics*, 13(9), 5049–5062. <https://doi.org/10.5194/acp-13-5049-2013>
- Laskin, A., Wietsma, T. W., Krueger, B. J., & Grassian, V. H. (2005). Heterogeneous chemistry of individual mineral dust particles with nitric acid: A combined CCSEM/EDX, ESEM, and ICP-MS study. *Journal of Geophysical Research: Atmospheres*, 110(D10).
<https://doi.org/10.1029/2004JD005206>
- Laskin, Alexander, Moffet, R. C., Gilles, M. K., Fast, J. D., Zaveri, R. A., Wang, B., Nigge, P., & Shutthanandan, J. (2012). Tropospheric chemistry of internally mixed sea salt and organic particles: Surprising reactivity of NaCl with weak organic acids. *Journal of Geophysical Research: Atmospheres*, 117(D15).
<https://doi.org/10.1029/2012JD017743>
- Levin, Z., Teller, A., Ganor, E., & Yin, Y. (2005). On the interactions of mineral dust, sea-salt particles, and clouds: A measurement and modeling study from the Mediterranean Israeli Dust Experiment campaign. *Journal of Geophysical Research: Atmospheres*, 110(D20).
<https://doi.org/10.1029/2005JD005810>
- Levin, Zev, Ganor, E., & Gladstein, V. (1996). The Effects of Desert Particles Coated with Sulfate on Rain Formation in the Eastern Mediterranean. *Journal of Applied Meteorology and Climatology*, 35(9), 1511–1523. [https://doi.org/10.1175/1520-0450\(1996\)035<1511:TEODPC>2.0.CO;2](https://doi.org/10.1175/1520-0450(1996)035<1511:TEODPC>2.0.CO;2)
- Li-Jones, X., & Prospero, J. M. (1998). Variations in the size distribution of non-sea-salt sulfate aerosol in the marine boundary layer at Barbados: Impact of African dust. *Journal of Geophysical Research: Atmospheres*, 103(D13), 16073–16084.
<https://doi.org/10.1029/98JD00883>
- Li, J., Pósfai, M., Hobbs, P. V., & Buseck, P. R. (2003). Individual aerosol particles from biomass burning in southern Africa: 2, Compositions and aging of inorganic particles. *Journal of Geophysical Research: Atmospheres*, 108(D13).
<https://doi.org/10.1029/2002JD002310>

- Li, W., Shao, L., Shi, Z., Chen, J., Yang, L., Yuan, Q., Yan, C., Zhang, X., Wang, Y., Sun, J., Zhang, Y., Shen, X., Wang, Z., & Wang, W. (2014). Mixing state and hygroscopicity of dust and haze particles before leaving Asian continent. *Journal of Geophysical Research: Atmospheres*, 119(2), 1044–1059. <https://doi.org/10.1002/2013JD021003>
- Li, Y., Zhou, Y., Guo, W., Zhang, X., Huang, Y., He, E., Li, R., Yan, B., Wang, H., Mei, F., Liu, M., & Zhu, Z. (2023). Molecular Imaging Reveals Two Distinct Mixing States of PM2.5 Particles Sampled in a Typical Beijing Winter Pollution Case. *Environmental Science & Technology*, 57(15), 6273–6283. <https://doi.org/10.1021/acs.est.2c08694>
- Ma, C.-J., Tohno, S., Kasahara, M., & Hayakawa, S. (2004). Properties of the size-resolved and individual cloud droplets collected in western Japan during the Asian dust storm event. *Atmospheric Environment*, 38(27), 4519–4529. <https://doi.org/10.1016/j.atmosenv.2004.05.032>
- Mahowald, N. (2011). Aerosol Indirect Effect on Biogeochemical Cycles and Climate. *Science*, 334(6057), 794–796. <https://doi.org/10.1126/science.1207374>
- Metzger, S., Mihalopoulos, N., & Lelieveld, J. (2006). Importance of mineral cations and organics in gas-aerosol partitioning of reactive nitrogen compounds: case study based on MINOS results. *Atmospheric Chemistry and Physics*, 6(9), 2549–2567. <https://doi.org/10.5194/acp-6-2549-2006>
- Myhre, G., & Stordal, F. (2001). Global sensitivity experiment of the radiative forcing due to mineral aerosols. *Journal of Geophysical Research*, 106, 18193–18204. <https://doi.org/10.1029/2000JD900536>
- Nenes, A., Krom, M. D., Mihalopoulos, N., Van Cappellen, P., Shi, Z., Bougiatioti, A., Zarmas, P., & Herut, B. (2011). Atmospheric acidification of mineral aerosols: a source of bioavailable phosphorus for the oceans. *Atmospheric Chemistry and Physics*, 11(13), 6265–6272. <https://doi.org/10.5194/acp-11-6265-2011>
- Olson, N.E., May, N.W., Kirpes, R.M., Watson, A.E., Hajny, K.D., Slade, J.H., Shepson, P.B., Stirm, B.H., Pratt, K.A., & Ault, A.P. (2019) Lake spray aerosol incorporated into Great Lakes Clouds. *ACS Earth & Space Chemistry*, 3, (12), 2765–2774.
- Pringle, K. J., Tost, H., Pozzer, A., Pöschl, U., & Lelieveld, J. (2010). Global distribution of the effective aerosol hygroscopicity parameter for CCN activation. *Atmospheric Chemistry and Physics*, 10(12), 5241–5255. <https://doi.org/10.5194/acp-10-5241-2010>
- Prospero, J M. (1968). atmospheric dust studies on Barbados. *Bulletin of the American Meteorological Society*, 49(6), 645–652. <https://doi.org/10.1175/1520-0477-49.6.645>
- Prospero, J. M., & Mayol-Bracero, O. L. (2013). Understanding the transport and impact of African dust on the Caribbean Basin. *Bulletin of the American Meteorological Society*, 94(9), 1329–1337. <https://doi.org/10.1175/BAMS-D-12-00142.1>
- Prospero, J. M. (1999). Long-range transport of mineral dust in the global atmosphere: Impact of African dust on the environment of the southeastern United States. *Proceedings of the National Academy of Sciences*, 96(7), 3396 LP – 3403. <https://doi.org/10.1073/pnas.96.7.3396>
- Prospero, J.M, Blades, E., Mathison, G., & Naidu, R. (2005). Interhemispheric transport of viable fungi and bacteria from Africa to the Caribbean with soil dust. *Aerobiologia*, 21(1), 1–19. <https://doi.org/10.1007/s10453-004-5872-7>
- Prospero, J. M, Delany, A. C., Delany, A. C., & Carlson, T. N. (2021). The Discovery of African Dust Transport to the Western Hemisphere and the Saharan Air Layer: A History. *Bulletin of the American Meteorological Society*, 102(6), E1239–E1260.

- <https://doi.org/10.1175/BAMS-D-19-0309.1>
- Quinn, P. K., Thompson, E. J., Coffman, D. J., Baidar, S., Bariteau, L., Bates, T. S., Bigorre, S., Brewer, A., de Boer, G., de Szoek, S. P., Drushka, K., Foltz, G. R., Intrieri, J., Iyer, S., Fairall, C. W., Gaston, C. J., Jansen, F., Johnson, J. E., Krüger, O. O., Marchbanks, R. D., Moran, K. P., Noone, D., Pezoa, S., Pincus, R., Plueddemann, A. J., Pöhlker, M. L., Pöschl, U., Quinones Melendez, E., Royer, H. M., Szczodrak, M., Thomson, J., Upchurch, L. M., Zhang, C., Zhang, D., & Zuidema, P. (2021). Measurements from the RV Ronald H. Brown and related platforms as part of the Atlantic Tradewind Ocean-Atmosphere Mesoscale Interaction Campaign (ATOMIC). *Earth Syst. Sci. Data*, 13(4), 1759–1790. <https://doi.org/10.5194/essd-13-1759-2021>
- Rickly, P. S., Guo, H., Campuzano-Jost, P., Jimenez, J. L., Wolfe, G. M., Bennett, R., Bourgeois, I., Crounse, J. D., Dibb, J. E., DiGangi, J. P., Diskin, G. S., Dollner, M., Gargulinski, E. M., Hall, S. R., Halliday, H. S., Hanisco, T. F., Hannun, R. A., Liao, J., Moore, R., Nault, B. A., Nowak, J. B., Peischl, J., Robinson, C. E., Ryerson, T., Sanchez, K. J., Schöberl, M., Soja, A. J., St. Clair, J. M., Thornhill, K. L., Ullmann, K., Wennberg, P. O., Weinzierl, B., Wiggins, E. B., Winstead, E. L., & Rollins, A. W. (2022). Emission factors and evolution of SO₂ measured from biomass burning in wildfires and agricultural fires. *Atmospheric Chemistry and Physics*, 22(23), 15603–15620. <https://doi.org/10.5194/acp-22-15603-2022>
- Rodriguez, S., Alastuey, A., Alonso-Pérez, S., Querol, X., Cuevas, E., Abreu-Afonso, J., Viana, M., Pérez, N., Pandolfi, M., & de la Rosa, J. (2011). Transport of desert dust mixed with North African industrial pollutants in the subtropical Saharan Air Layer. *Atmospheric Chemistry & Physics*, 11, 6663–6685.
- Rodríguez, S., Prospero, J.M., López-Darias, J., García-Alvarez, M.-I., Zuidema, P., Nava, S., Lucarelli, F., Gaston, C.J., Galindo, L., & Sosa, E. (2021). Tracking the changes of iron solubility and air pollutants traces as African dust transits the Atlantic in the Saharan dust outbreaks. *Atmospheric Environment*, 246, <https://doi.org/10.1016/j.atmosenv.2020.118092>.
- Rosenfeld, D., Rudich, Y., & Lahav, R. (2001). Desert dust suppressing precipitation: A possible desertification feedback loop. *Proceedings of the National Academy of Sciences*, 98(11), 5975 LP – 5980. <https://doi.org/10.1073/pnas.101122798>
- Royer, H. M., Pöhlker, M. L., Krüger, O., Blades, E., Sealy, P., Lata, N. N., Cheng, Z., China, S., Ault, A. P., Quinn, P. K., Zuidema, P., Pöhlker, C., Pöschl, U., Andreae, M., & Gaston, C. J. (2023). African smoke particles act as cloud condensation nuclei in the wintertime tropical North Atlantic boundary layer over Barbados. *Atmospheric Chemistry and Physics*, 23(2), 981–998. <https://doi.org/10.5194/acp-23-981-2023>
- Ryder, C. L., Marenco, F., Brooke, J. K., Estelles, V., Cotton, R., Formenti, P., McQuaid, J. B., Price, H. C., Liu, D., Ausset, P., Rosenberg, P. D., Taylor, J. W., Choularton, T., Bower, K., Coe, H., Gallagher, M., Crosier, J., Lloyd, G., Highwood, E. J., & Murray, B. J. (2018). Coarse-mode mineral dust size distributions, composition and optical properties from AER-D aircraft measurements over the tropical eastern Atlantic. *Atmospheric Chemistry and Physics*, 18(23), 17225–17257. <https://doi.org/10.5194/acp-18-17225-2018>
- Savoie, D L, & Prospero, J. M. (1982). Particle size distribution of nitrate and sulfate in the marine atmosphere. *Geophysical Research Letters*, 9(10), 1207–1210. <https://doi.org/https://doi.org/10.1029/GL009i010p01207>
- Savoie, Dennis L, Arimoto, R., Keene, W. C., Prospero, J. M., Duce, R. A., & Galloway, J. N. (2002). Marine biogenic and anthropogenic contributions to non-sea-salt sulfate in the marine boundary layer over the North Atlantic Ocean. *Journal of Geophysical Research*:

- Atmospheres*, 107(D18), AAC 3-1-AAC 3-21.
<https://doi.org/https://doi.org/10.1029/2001JD000970>
- Shen, H., Peters, T. M., Casuccio, G. S., Lersch, T. L., West, R. R., Kumar, A., Kumar, N., & Ault, A. P. (2016). Elevated Concentrations of Lead in Particulate Matter on the Neighborhood-Scale in Delhi, India As Determined by Single Particle Analysis. *Environmental Science & Technology*, 50(10), 4961–4970.
<https://doi.org/10.1021/acs.est.5b06202>
- Shi, Z., Zhang, D., Hayashi, M., Ogata, H., Ji, H., & Fujiie, W. (2008). Influences of sulfate and nitrate on the hygroscopic behaviour of coarse dust particles. *Atmospheric Environment*, 42(4), 822–827. <https://doi.org/https://doi.org/10.1016/j.atmosenv.2007.10.037>
- Sobanska, S., Coeur, C., Maenhaut, W., & Adams, F. (2003). SEM-EDX Characterisation of Tropospheric Aerosols in the Negev Desert (Israel). *Journal of Atmospheric Chemistry*, 44(3), 299–322. <https://doi.org/10.1023/A:1022969302107>
- Sokolik, I. N., Winker, D. M., Bergametti, G., Gillette, D. A., Carmichael, G., Kaufman, Y. J., Gomes, L., Schuetz, L., & Penner, J. E. (2001). Introduction to special section: Outstanding problems in quantifying the radiative impacts of mineral dust. *Journal of Geophysical Research: Atmospheres*, 106(D16), 18015–18027.
<https://doi.org/https://doi.org/10.1029/2000JD900498>
- Spokes, L. J., & Jickells, T. D. (1995). Factors controlling the solubility of aerosol trace metals in the atmosphere and on mixing into seawater. *Aquatic Geochemistry*, 1(4), 355–374.
<https://doi.org/10.1007/BF00702739>
- Stein, A.F., Draxler, R.R., Rolph, G.D., Stunder, B.J.B., Cohen, M.D., & Ngan, F. (2015). NOAA's HYSPLIT atmospheric transport and dispersion modeling system. *Bulletin of the American Meteorological Society*, 96(12), 2059–2077.
- Stevens, B., Bony, S., Farrell, D., Ament, F., Blyth, A., Fairall, C., Karstensen, J., Quinn, P. K., Speich, S., Acquistapace, C., Aemisegger, F., Albright, A. L., Bellenger, H., Bodenschatz, E., Caesar, K.-A., Chewitt-Lucas, R., de Boer, G., Delanoë, J., Denby, L., Ewald, F., Fildier, B., Forde, M., George, G., Gross, S., Hagen, M., Hausold, A., Heywood, K. J., Hirsch, L., Jacob, M., Jansen, F., Kinne, S., Klocke, D., Kölling, T., Konow, H., Lothon, M., Mohr, W., Naumann, A. K., Nuijens, L., Olivier, L., Pincus, R., Pöhlker, M., Reverdin, G., Roberts, G., Schnitt, S., Schulz, H., Siebesma, A. P., Stephan, C. C., Sullivan, P., Touzé-Peiffer, L., Vial, J., Vogel, R., Zuidema, P., Alexander, N., Alves, L., Arixi, S., Asmath, H., Bagheri, G., Baier, K., Bailey, A., Baranowski, D., Baron, A., Barrau, S., Barrett, P. A., Batier, F., Behrendt, A., Bendinger, A., Beucher, F., Bigorre, S., Blades, E., Blossey, P., Bock, O., Böing, S., Bosser, P., Bourras, D., Bouruet-Aubertot, P., Bower, K., Branellec, P., Branger, H., Brennek, M., Brewer, A., Brilouet, P.-E., Brüggmann, B., Buehler, S. A., Burke, E., Burton, R., Calmer, R., Canonici, J.-C., Carton, X., Cato Jr., G., Charles, J. A., Chazette, P., Chen, Y., Chilinski, M. T., Choularton, T., Chuang, P., Clarke, S., Coe, H., Cornet, C., Coutris, P., Couvreur, F., Crewell, S., Cronin, T., Cui, Z., Cuypers, Y., Daley, A., Damerell, G. M., Dauhut, T., Deneke, H., Desbios, J.-P., Dörner, S., Donner, S., Douet, V., Drushka, K., Dütsch, M., Ehrlich, A., Emanuel, K., Emmanouilidis, A., Etienne, J.-C., Etienne-Leblanc, S., Faure, G., Feingold, G., Ferrero, L., Fix, A., Flamant, C., Flatau, P. J., Foltz, G. R., Forster, L., Furtuna, I., Gadian, A., Galewsky, J., Gallagher, M., Gallimore, P., Gaston, C., Gentemann, C., Geyskens, N., Giez, A., Gollop, J., Gouirand, I., Gourbeyre, C., de Graaf, D., de Groot, G. E., Grosz, R., Güttler, J., Gutleben, M., Hall, K., Harris, G., Helfer, K. C., Henze, D., Herbert, C., Holanda, B., Ibanez-Landeta, A.,

982 Intrieri, J., Iyer, S., Julien, F., Kalesse, H., Kazil, J., Kellman, A., Kidane, A. T., Kirchner,
 983 U., Klingebiel, M., Körner, M., Kremper, L. A., Kretzschmar, J., Krüger, O., Kumala, W.,
 984 Kurz, A., L'Hégaret, P., Labaste, M., Lachlan-Cope, T., Laing, A., Landschützer, P., Lang,
 985 T., Lange, D., Lange, I., Laplace, C., Lavik, G., Laxenaire, R., Le Bihan, C., Leandro, M.,
 986 Lefevre, N., Lena, M., Lenschow, D., Li, Q., Lloyd, G., Los, S., Losi, N., Lovell, O.,
 987 Luneau, C., Makuch, P., Malinowski, S., Manta, G., Marinou, E., Marsden, N., Masson, S.,
 988 Maury, N., Mayer, B., Mayers-Als, M., Mazel, C., McGeary, W., McWilliams, J. C., Mech,
 989 M., Mehlmann, M., Meroni, A. N., Mieslinger, T., Minikin, A., Minnett, P., Möller, G.,
 990 Morfa Avalos, Y., Muller, C., Musat, I., Napoli, A., Neuberger, A., Noisel, C., Noone, D.,
 991 Nordsiek, F., Nowak, J. L., Oswald, L., Parker, D. J., Peck, C., Person, R., Philippi, M.,
 992 Plueddemann, A., Pöhlker, C., Pörtge, V., Pöschl, U., Pologne, L., Posyniak, M., Prange,
 993 M., Quiñones Meléndez, E., Radtke, J., Ramage, K., Reimann, J., Renault, L., Reus, K.,
 994 Reyes, A., Ribbe, J., Ringel, M., Ritschel, M., Rocha, C. B., Rochetin, N., Röttenbacher, J.,
 995 Rollo, C., Royer, H., Sadoulet, P., Saffin, L., Sandiford, S., Sandu, I., Schäfer, M.,
 996 Schemann, V., Schirmacher, I., Schlenczek, O., Schmidt, J., Schröder, M.,
 997 Schwarzenboeck, A., Sealy, A., Senff, C. J., Serikov, I., Shohan, S., Siddle, E., Smirnov, A.,
 998 Späth, F., Spooner, B., Stolla, M. K., Szkółka, W., de Szoeke, S. P., Tarot, S., Tetoni, E.,
 999 Thompson, E., Thomson, J., Tomassini, L., Totems, J., Ubele, A. A., Villiger, L., von Arx,
 1000 J., Wagner, T., Walther, A., Webber, B., Wendisch, M., Whitehall, S., Wiltshire, A., Wing,
 1001 A. A., Wirth, M., Wiskandt, J., Wolf, K., Worbes, L., Wright, E., Wulfmeyer, V., Young,
 1002 S., Zhang, C., Zhang, D., Ziemer, F., Zinner, T., & Zöger, M. (2021). EUREC4A. *Earth*
 1003 *Syst. Sci. Data*, 13(8), 4067–4119. <https://doi.org/10.5194/essd-13-4067-2021>
 1004 Stockdale, A., Krom, M. D., Mortimer, R. J. G., Benning, L. G., Carslaw, K. S., Herbert, R. J.,
 1005 Shi, Z., Myriokefalitakis, S., Kanakidou, M., & Nenes, A. (2016). Understanding the nature
 1006 of atmospheric acid processing of mineral dusts in supplying bioavailable phosphorus to the
 1007 oceans. *Proceedings of the National Academy of Sciences*, 113(51), 14639–14644.
 1008 <https://doi.org/10.1073/pnas.1608136113>
 1009 Sullivan, R. C., Guazzotti, S. A., Sodeman, D. A., & Prather, K. A. (2007). Direct observations
 1010 of the atmospheric processing of Asian mineral dust. *Atmospheric Chemistry and Physics*,
 1011 7(5), 1213–1236. <https://doi.org/10.5194/acp-7-1213-2007>
 1012 Sullivan, R. C., Moore, M. J. K., Petters, M. D., Kreidenweis, S. M., Roberts, G. C., & Prather,
 1013 K. A. (2009). Effect of chemical mixing state on the hygroscopicity and cloud nucleation
 1014 properties of calcium mineral dust particles. *Atmospheric Chemistry and Physics*, 9(10),
 1015 3303–3316. <https://doi.org/10.5194/acp-9-3303-2009>
 1016 Sullivan, R. C., & Prather, K. A. (2007). Investigations of the diurnal cycle and mixing state of
 1017 oxalic acid in individual particles in Asian aerosol outflow. *Environmental Science and*
 1018 *Technology*, 41(23), 8062–8069. <https://doi.org/10.1021/es071134g>
 1019 Tang, M. J., Cziczo, D. J., and Grassian, V. H. (2016) Interactions of water with mineral dust
 1020 aerosol: Water adsorption, hygroscopicity, cloud condensation and ice nucleation.
 1021 *Chemical Reviews*, 116, 4205–4259.
 1022 Tegen, I. (2003). Modeling the mineral dust aerosol cycle in the climate system. *Quaternary*
 1023 *Science Reviews*, 22(18), 1821–1834. [https://doi.org/https://doi.org/10.1016/S0277-](https://doi.org/https://doi.org/10.1016/S0277-3791(03)00163-X)
 1024 [3791\(03\)00163-X](https://doi.org/https://doi.org/10.1016/S0277-3791(03)00163-X)
 1025 Tsamalis, C., Chédin, A., Pelon, J., & Capelle, V. (2013). The seasonal vertical distribution of
 1026 the Saharan Air Layer and its modulation by the wind. *Atmos. Chem. Phys.*, 13(22), 11235–
 1027 11257. <https://doi.org/10.5194/acp-13-11235-2013>

- Ullerstam, M., Vogt, R., Langer, S., & Ljungström, E. (2002). The kinetics and mechanism of SO₂ oxidation by O₃ on mineral dust. *Physical Chemistry Chemical Physics*, 4(19), 4694–4699. <https://doi.org/10.1039/B203529B>
- van Herpen, M.M.J.W., Li, Q., Saiz-Lopez, A., Liisberg, J.B., Röckmann, T., Cuevas, C.A., Fernandez, R.P., Mak, J.E., Mahowald, N.M., Hess, P., Meidan, D., Stuut, J.-B.W., & Johnson, M.S. (2023). Photocatalytic chlorine atom production on mineral dust-sea spray aerosols over the North Atlantic. *Proceedings of the National Academy of Sciences*, 120(31), <https://doi.org/10.1073/pnas.2303974120>.
- Weinzierl, B., Ansmann, A., Prospero, J. M., Althausen, D., Benker, N., Chouza, F., Dollner, M., Farrell, D., Fomba, W. K., Freudenthaler, V., Gasteiger, J., Groß, S., Haarig, M., Heinold, B., Kandler, K., Kristensen, T. B., Mayol-Bracero, O. L., Müller, T., Reitebuch, O., Sauer, D., Schäfler, A., Schepanski, K., Spanu, A., Tegen, I., Toledano, C., & Walser, A. (2017). The Saharan Aerosol Long-Range Transport and Aerosol–Cloud-Interaction Experiment: Overview and Selected Highlights. *Bulletin of the American Meteorological Society*, 98(7), 1427–1451. <https://doi.org/10.1175/BAMS-D-15-00142.1>
- Wu, Z., Birmili, W., Poulain, L., Wang, Z., Merkel, M., Fahlbusch, B., van Pinxteren, D., Herrmann, H., & Wiedensohler, A. (2013). Particle hygroscopicity during atmospheric new particle formation events: implications for the chemical species contributing to particle growth. *Atmospheric Chemistry and Physics*, 13(13), 6637–6646. <https://doi.org/10.5194/acp-13-6637-2013>
- Wurzler, S., Reisin, T. G., & Levin, Z. (2000). Modification of mineral dust particles by cloud processing and subsequent effects on drop size distributions. *Journal of Geophysical Research: Atmospheres*, 105(D4), 4501–4512. <https://doi.org/10.1029/1999JD900980>
- Zhang, H.H., Li, R., Huang, C.P., Li, X.F., Dong, S.W., Wang, F., Li, T.T., Chen, Y.Z., Zhang, G.H., Ren, Y., Chen, Q.C., Huang, R.J., Chen, S.Y., Xue, T., Wang, X.M., & Tang, M.J. (2023) Seasonal variation of aerosol iron solubility in coarse and fine particles at an inland city in northwestern China. *Atmospheric Chemistry & Physics*, 23, 3543–3559.
- Zuidema, P., Alvarez, C., Kramer, S. J., Custals, L., Izaguirre, M., Sealy, P., Prospero, J. M., & Blades, E. (2019). Is Summer African Dust Arriving Earlier to Barbados? The Updated Long-Term In Situ Dust Mass Concentration Time Series from Ragged Point, Barbados, and Miami, Florida. *Bulletin of the American Meteorological Society*, 100(10), 1981–1986. <https://doi.org/10.1175/BAMS-D-18-0083.1>